Review

Bandgap Science for Organic Solar Cells

Masahiro Hiramoto [1,2,]*, **Masayuki Kubo** [1,2], **Yusuke Shinmura** [1,2], **Norihiro Ishiyama** [1,2], **Toshihiko Kaji** [1,2], **Kazuya Sakai** [3], **Toshinobu Ohno** [4] **and Masanobu Izaki** [2,5]

[1] Institute for Molecular Science, 5-1 Higashiyama, Myodaiji, Okazaki, Aichi 444-8787, Japan; E-Mails: kubo@ims.ac.jp (M.K.); shinmura@ims.ac.jp (Y.S.); ishiyama@ims.ac.jp (N.I.); kaji@ims.ac.jp (T.K.)

[2] JST, CREST, 5, Sanbancho, Chiyoda-ku, Tokyo 102-0075, Japan

[3] Graduate School of Engineering, Osaka University, Yamadaoka, Suita, Osaka 565-0871, Japan; E-Mail: kazuya_sakai@gg.nitto.co.jp

[4] Osaka Municipal Technical Research Institute, 1-6-50 Morinomiya, Joto-ku, Osaka 536-8553, Japan; E-Mail: ohno@omtri.or.jp

[5] Department of Production System Engineering, Toyohashi University of Technology, Tempaku-cho, Toyohashi, Aichi 441-8580, Japan; E-Mail: m-izaki@me.tut.ac.jp

* Author to whom correspondence should be addressed; E-Mail: hiramoto@ims.ac.jp; Tel./Fax: +81-564-59-5536.

Abstract: The concept of bandgap science of organic semiconductor films for use in photovoltaic cells, namely, high-purification, *pn*-control by doping, and design of the built-in potential based on precisely-evaluated doping parameters, is summarized. The principle characteristics of organic solar cells, namely, the exciton, donor (D)/acceptor (A) sensitization, and *p-i-n* cells containing co-deposited and D/A molecular blended *i*-interlayers, are explained. 'Seven-nines' (7N) purification, together with phase-separation/cystallization induced by co-evaporant 3rd molecules allowed us to fabricate 5.3% efficient cells based on 1 µm-thick fullerene:phthalocyanine (C_{60}:H_2Pc) co-deposited films. *pn*-control techniques enabled by impurity doping for both single and co-deposited films were established. The carrier concentrations created by doping were determined by the Kelvin band mapping technique. The relatively high ionization efficiency of 10% for doped organic semiconductors can be explained by the formation of charge transfer (CT)-complexes between the dopants and the organic semiconductor molecules. A series of fundamental junctions, such as Schottky junctions, *pn*-homojunctions, p^+, n^+-organic/metal ohmic junctions, and n^+-organic/

p^+-organic ohmic homojunctions, were fabricated in both single and co-deposited organic semiconductor films by impurity doping alone. A tandem cell showing 2.4% efficiency was fabricated in which the built-in electric field was designed by manipulating the doping.

Keywords: organic solar cell; doping; bandgap science; seven-nines purification; phase-separation; *pn*-control; co-deposited film; Kelvin band mapping; carrier concentration; ionization efficiency; built-in potential design; *pn*-homojunction; metal/organic ohmic junction; organic/organic ohmic homojunction; tandem cell

1. Introduction

Organic solar cells consisting of vacuum-deposited small-molecular thin films have been intensively studied [1–3], following the two-layer cell reported by Tang [4]. In 1991, the author proposed *p-i-n* organic solar cells in which the *i*-interlayer is a co-deposited film of *p*- and *n*-type organic semiconductors [5,6]. This is the first organic solar cell having a molecular blend, *i.e.*, the so-called bulk heterojunction [7].

Recently, we have been focused on the establishment of "bandgap science for organic solar cells". We believe that the following features are indispensable. (a) Organic semiconductors purified to sub-ppm level, at least seven nines (7N; 0.1 ppm), should be used; (b) A ppm-level doping technique should be developed; (c) Every individual organic semiconductor should be capable of displaying both *n*- and *p*-type characteristics by impurity doping alone, *i.e.*, complete *pn*-control should be developed; (d) Unintentional and uncontrollable doping by oxygen and water from air should be completely eliminated; (e) The doping technique should be applicable not only to single organic semiconductor films, but also to co-deposited films consisting of two kinds of organic semiconductors.

pn-control by doping are indispensable for the solid-state physics of inorganic semiconductors. It is so-called "bandgap engineering". In the case of organic semiconductors, their genuine potential has been hidden for a long time by the unintentional and unknown impurity contamination typically by oxygen from air. However, the authors have a strong conviction that the organic semiconductors should also be able to be treated similar to the inorganic semiconductors. Simultaneously, the authors strongly expect that the unknown physical phenomena, particular to organic semiconductors will be discovered during the course of research to establish the solid-state physics for organic semiconductors. From these standpoints of view, the authors chose the term "bandgap science". *pn*-control of co-deposited films consisting of D/A organic semiconductors is one of the spin-off of "bandgap science" and particular to organic semiconductors.
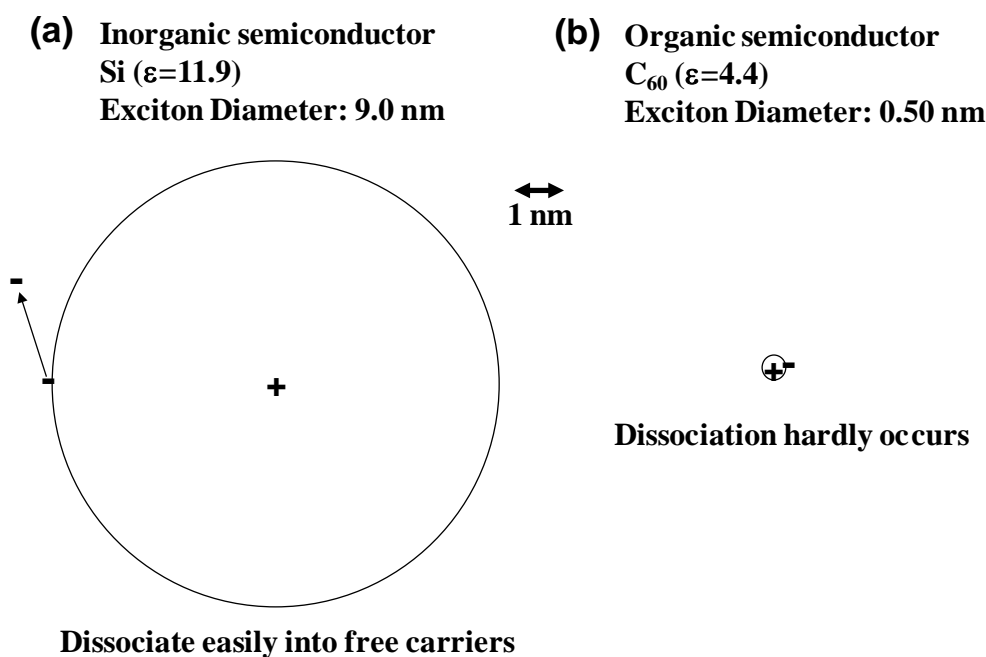
In this paper we will first summarize the fundamental principles of organic solar cells, such as the exciton, donor (D)/acceptor (A) sensitization, *p-i-n* cells containing a co-deposited *i*-interlayer, and nanostructure design of co-deposited layers. Next, factors influencing bandgap science for organic solar cells, such as 'seven-nines' purification, *pn*-control by ppm-level doping for both single and for co-deposited organic semiconductor films, and built-in potential design based on precise evaluation of doping parameters, are summarized.

2. Principles

2.1. Exciton

The dissociation of photogenerated electron-hole pairs (excitons) is a key factor for carrier generation in organic semiconductors. Exciton dissociation is affected by the relative permittivity of a solid (ε) based on the Coulomb's law; $F = (1/4\pi\varepsilon\varepsilon_0)(q_1q_2/r_2)$ [8]. Here, ε_0, q_1, q_2, and r are the absolute permittivity, the elementary charges, and the distance between charges. In a solid having a small value of ε, the positive and negative charges experience strong attractive forces. On the contrary, in a solid having a large value of ε, the positive and negative charges experience relatively weak attractive forces. Inorganic semiconductors have large values for ε. For example, Si has a large ε value of 11.9 and the exciton has a large diameter of 9.0 nm and is delocalized over about 10^4 Si atoms (Figure 1a) [9]. This Wannier-type exciton immediately dissociates to a free electron and a hole from thermal energy at room temperature and generates photocurrent. On the other hand, organic semiconductors have small values for ε. For example, C_{60} has small ε value of 4.4 and the exciton has a very small diameter of 0.50 nm and is localized on a single C_{60} molecule (Figure 1b). These Frenkel-type excitons are hardly dissociated to free electrons and holes by thermal energy of room temperature and can easily relax to the ground state (Figure 2a). Therefore, organic semiconductors can generate few photocarriers. This is the reason why the organic solar cells that were fabricated before the work of Tang [4] showed extremely low photocurrents, of the order of nano- to micro-amperes.

Figure 1. Size of excitons for an inorganic semiconductor (Si) and an organic semiconductor (C_{60}). The former is Wannier-type and easily dissociates to free carriers. The latter is Frenkel-type and hardly dissociates to free carriers.
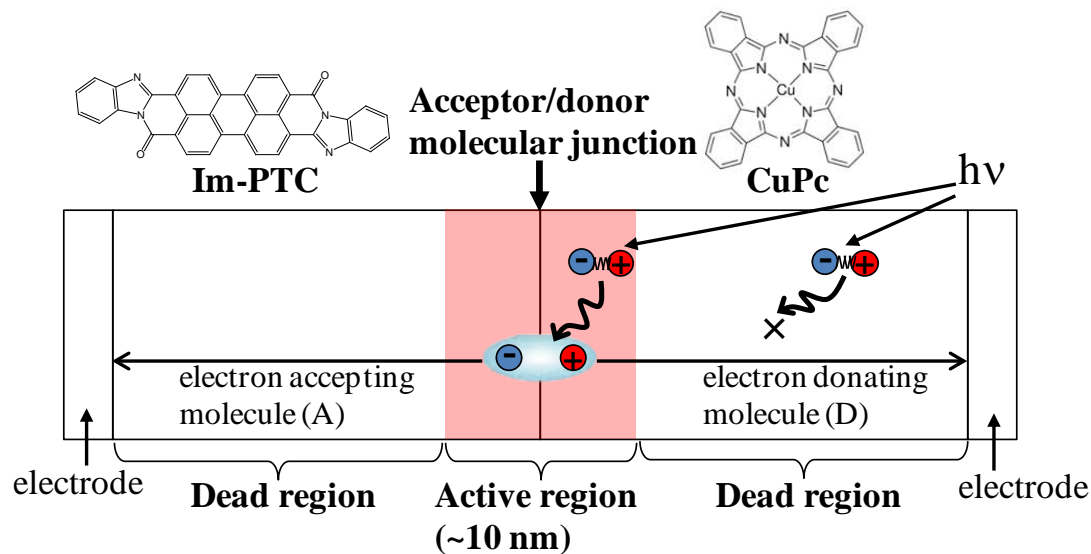

(a) **Inorganic semiconductor**
Si (ε=11.9)
Exciton Diameter: 9.0 nm

(b) **Organic semiconductor**
C_{60} (ε=4.4)
Exciton Diameter: 0.50 nm

1 nm

Dissociation hardly occurs

Dissociate easily into free carriers

Figure 2. Carrier generation in organic semiconductors. (**a**) Single molecular solids; (**b**) Donor (D)/acceptor (A) sensitization of carrier generation by the mixing of two kinds of organic semiconductor molecules. Efficient free carrier generation occurs from the charge transfer (CT) exciton.
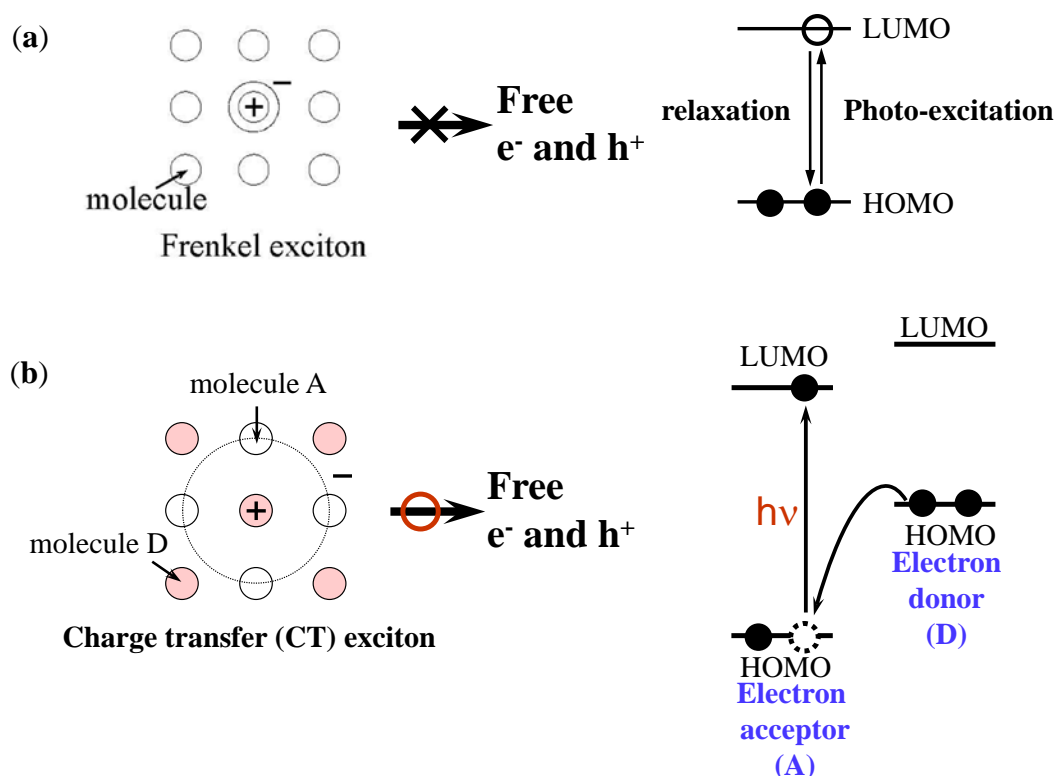
Today's organic solar cells have overcome the above problem by combining two kinds of organic semiconductors. When an electron-donating molecule (D) and an electron-accepting molecule (A), for which the energetic relationship of the highest occupied molecular orbital (HOMO) and the lowest unoccupied molecular orbital (LUMO), are shifted in parallel with each other and are contacted or mixed, then a charge transfer (CT) exciton is formed in which the positive and negative charges are separated on the neighboring D and A molecules due to photoinduced electron transfer (Figure 2b). This CT exciton can dissociate to a free electron and a hole due to thermal energy of room temperature. By utilizing this donor-acceptor (D/A) sensitization, organic semiconductors became capable of generating photocurrents of significant magnitude; of the order of milli-amperes.

A two-layer organic solar cell (Figure 3) [4] utilizes D/A sensitization at the heterojunction. The width of the photoactive region (shaded red) is, however, limited to around 10 nm in the vicinity of the heterojunction due to the extremely small exciton diffusion length of only several nm [10,11]. Thus, when the thickness of the organic layers increases, a dead region that does not generate photocurrent and but absorbs incident solar light develops in front of the active region and, as a result, the magnitude of the photocurrent is severely suppressed. Taking into account the observation that a 10 nm-thick organic film can only absorb a small part of the incident solar light, then in order to increase the efficiency of organic solar cells, the severely contradictory condition, namely, "the whole of the incident solar light shall be absorbed by only a 10 nm-thick active layer", should be satisfied.

Figure 3. Schematic illustration of a two-layer cell composed of perylene pigment (Im-PTC) acting as an acceptor molecule (A) and copper phthalocyanine (CuPc) acting as a donor molecule (D). Photocurrent is generated only in the active region (shaded red) close to the heterojunction and all other parts of organic films act as a dead region.


2.2. Co-Deposited Layer

In order to overcome this contradiction, in 1991, the authors proposed *p-i-n* organic solar cells in which the *i*-interlayer is a co-deposited film composed of *p*- and *n*-type organic semiconductors (Figure 4a) [5,6]. The original concept is that the positive and negative charges from ionized donors and acceptors in *n*-type and *p*-type organic semiconductors, respectively, are compensated by each other, and the resulting co-deposited interlayer behaves like an intrinsic semiconductor. From the standpoint of built-in potential formation in a molecular solid, the built-in electric field is distributed across an *i*-interlayer sandwiched by *n*- and *p*-layers, similar to the case of amorphous silicon incorporating a *p-i-n* junction (Figure 4b). From the standpoint of photocarrier generation occurring at the molecular-level, there are D/A molecular contacts acting as photocarrier generation sites due to the D/A sensitization in the whole of the bulk of the *i*-codeposited layer.

In 1991, the terms *p*-type and *n*-type implied the nature induced by unintentional and uncontrolled doping. The *p*- and *n*-type natures of phthalocyanine and perylene pigments (Figure 3) were induced by unidentified acceptor and donor impurities respectively, and the electron donating molecules (D) and the accepting molecules (A) were recognized as usually showing *p*- and *n*-type natures. It should be noted that the recent *pn*-control technique mentioned in Sections 5 and 6 is based on intentional and controlled impurity doping.

The 'molecular blend' structure became indispensable for organic solar cells. In 1995, a blended junction, *i.e.*, a "bulk heterojunction", was proposed by Heeger's group for the polymer solar cell [7]. Fundamentally, an *i*-codeposited layer has the physical meaning that, by transmitting the incident light through a vast number of heterointerfaces, the severe contradicting conditions, *i.e.*, "the whole of the incident solar light shall be absorbed by only an extremely thin active layer", can be satisfied.

Figure 4. (**a**) Concept of *p-i-n* cell. A mixed *i*-layer co-deposited with *n*- and *p*-type semiconductors is sandwiched between respective *p*- and *n*-type layers. The entire bulk of the *i*-layer acts as an active layer for photocarrier generation; (**b**) Energy structure of the *p-i-n* cell.
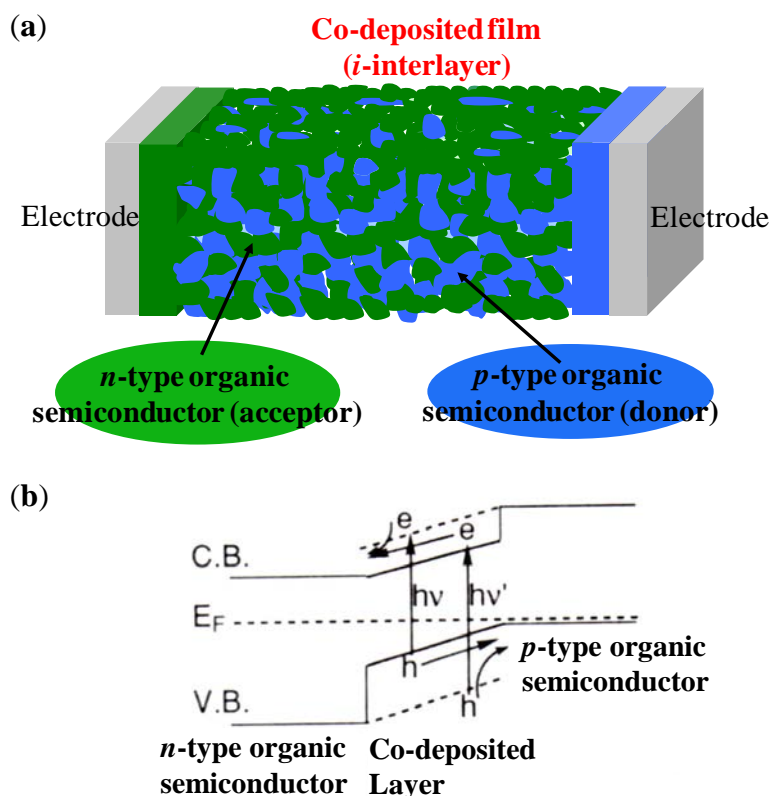

3. Nanostructure Design

3.1. Vertical Superlattice Structure

Even if excitonic dissociation occurs, nanostructure control of co-deposited films, *i.e.*, a formation route for electrons and holes generated by excitonic dissociation, is indispensable to extract a significant portion of the photogenerated charges to the external circuit. An ideal nanostructure is the 'vertical superlattice' structure (Figure 5b) [11]. This structure enables the efficient dissociation of photogenerated excitons at the D/A interfaces within the exciton diffusion length (5–10 nm) and the transport of electrons and holes to the respective electrodes.

Figure 5. (**a**) Co-evaporant 3rd molecule introduction. The balls, plates, and sticks correspond to C_{60}, H_2Pc, and 3rd molecules, respectively; (**b**) Vertical superlattice structure. Cross sectional SEM images of C_{60}:H_2Pc co-deposited films without (**c**) and with (**d**) 3rd molecule. Phase-separation and crystallization occurs by introducing co-evaporant 3rd molecule.
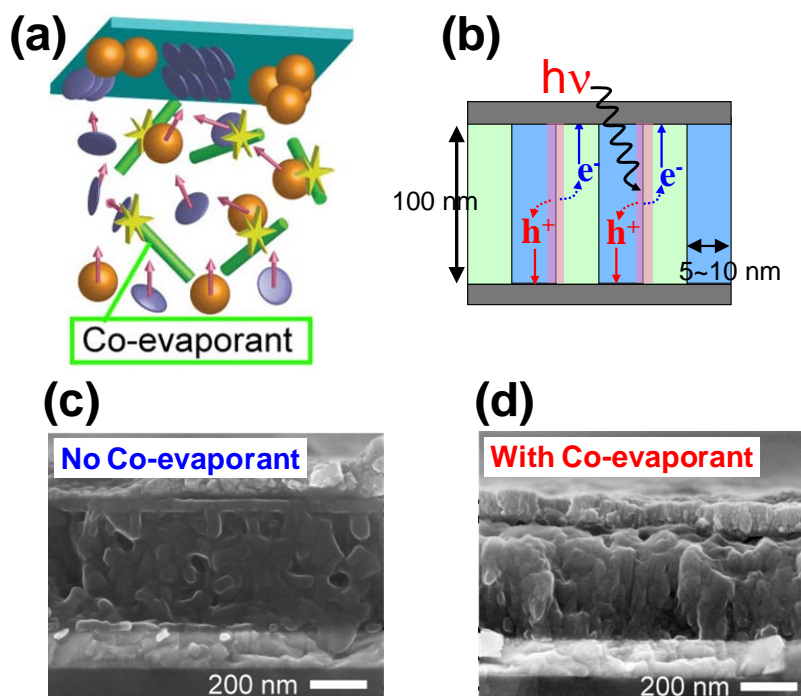
3.2. Co-Evaporant 3rd Molecules

Recently, we developed a fabrication method for a nanostructure similar to Figure 5b by using co-evaporant 3rd molecules that act as a solvent during vacuum deposition [12]. By introducing co-evaporant 3rd molecules onto a substrate heated to +80 °C during film growth, phase-separated and crystallized co-deposited films that improve carrier transport can be fabricated (Figure 5a). The 3rd molecules collide with C_{60} and H_2Pc and decrease the density of the crystalline nucleation sites on the surface and promote the crystallization/phase-separation process. The 3rd molecules are not left in the co-deposited films at elevated substrate temperatures. Columnar structure (Figure 5b) composed of benzoporphyrin and silylmethylfullerene was also fabricated by Matsuo *et al.* [13] and it was developed to commercialized organic solar cells by Mitsubishi Chemical.

Figure 5c,d show cross-sectional SEM images of a C_{60}:H_2Pc (fullerene:metal-free phthalocyanine) co-deposited film. Without the 3rd molecules, an amorphous smooth cross-section was observed for the molecular-level mixture of C_{60} and H_2Pc (Figure 5c). On the other hand, with the 3rd molecules, a columnar structure of phase-separated and crystallized material (Figure 5d) similar to the ideal vertical superlattice (Figure 5b) was formed. The improved crystallinity produced by introducing the 3rd molecules was confirmed by UV-Vis absorption spectra and X-ray diffraction analyses. Photocurrent enhancement was observed, particularly for relatively thick (>400 nm) co-deposited films having greater light absorption (see Section 4). A striking enhancement in photocurrent generation is achieved in organic solar cells without exception, based on a variety of co-deposited films such as H_2Pc:C_{60},

PbPc:C_{60}, AlClPc:C_{60}, and rubrene:C_{60}. As 3rd molecules, more than 10 kinds of low vapor pressure liquids, such as polydimethylsiloxane (PDMS) and alkyldiphenylether (ADE), can be used. Since ADE is a typical diffusion pump oil, the present effects can often be observed for co-deposition using a chamber evacuated by a diffusion pump (see Section 4). We believe that this method is generally applicable for growing high-quality phase-separated/crystalline co-deposited films by vacuum deposition.

4. Seven-Nines (7N) Purification

4.1. Single-Crystal Sublimation

First, in order to establish bandgap science for organic solar cells, we focused on the high purification of organic semiconductors. Conventional *p-i-n* cells (Section 2.2) [5,6] incorporating a quasi-vertical superlattice (Sections 3.1 and 3.2) [12] were used to evaluate the effects of high-purification.

Based on an analogy with inorganic Si, which is usually purified to eleven-nines (11N), the purity of organic semiconductors needs to at least reach the sub-ppm level in order to draw out their essential nature. Based on the above consideration, a more rigorous purification method was applied to organic semiconductors. Conventionally, organic semiconductors are purified by the 'train sublimation' method under vacuum [14] and the purified samples are obtained as a powder. Alternatively, when the sublimation is performed at 1 atm, the purified samples are obtained as single crystals that are of extremely high purity due to gas convection [15].

Figure 6a shows a photograph of C_{60} crystals purified by single-crystal sublimation [15]. Crystal growth was performed in a quartz tube surrounded by a three-zone furnace system (Epitech Co., Ltd., Kyoto, Japan) under flowing N_2 at 1 atm. The C_{60} sample was set at 720 °C and single crystals with sizes exceeding 2 mm $\times$ 2 mm were grown at around 500 °C. X-ray diffraction of the obtained crystals showed precise agreement with the reported crystal structure of C_{60}. The obtained C_{60} crystals were used in the next single-crystal sublimation process.

Figure 6. (**a**) Photograph of 7N-C_{60} single crystals; (**b**) Structure of organic *p-i-n* solar cell. The C_{60}:H_2Pc co-deposited layer (thickness: X nm) having a quasi-vertical superlattice structure (Figure 5b,d) is sandwiched between *p*-type H_2Pc and *n*-type NTCDA.


(**a**) (**b**)
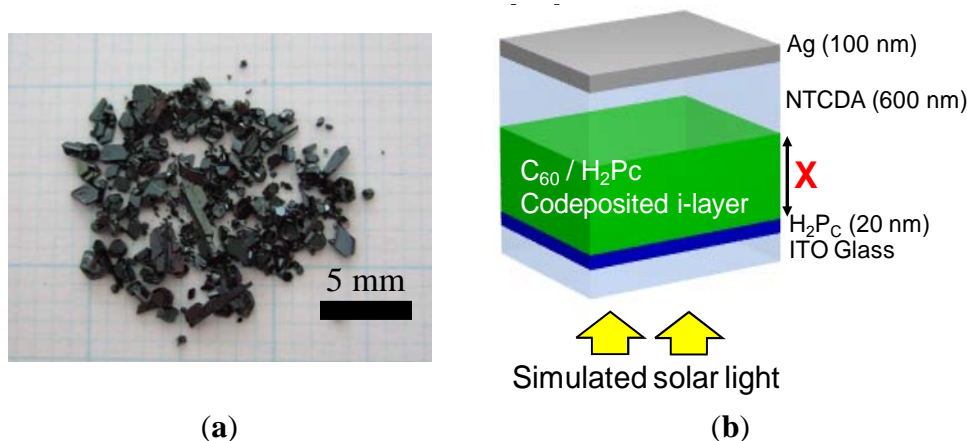
## 4.2. One Micrometer-Thick Co-Deposition Cells

Highly purified organic semiconductors produced by single-crystal sublimation were incorporated in *p-i-n* cells (Figure 6b) (Section 2.2, Figure 4). A *p*-type H_2Pc layer (20 nm), a co-deposited $C_{60}:H_2Pc$ *i*-interlayer, and an *n*-type layer of naphthalene tetracarboxylic anhydride (NTCDA) were successively deposited by vacuum evaporation at 1×10^{-3} Pa using a diffusion pump (VPC-260, ULVAC) onto an indium tin oxide (ITO) glass substrate pre-treated in an air plasma. The thick NTCDA layer (600 nm) also acts as a transparent protection layer that prevents electrical shorting of the cells due to metal migration into the organic film during metal deposition [16,17]. The co-deposition was performed on a substrate heated to +80 °C. The optimized $C_{60}:H_2Pc$ ratio was 1.13:1. ADE, which acted as a co-evaporant 3rd molecule (Section 3.2), was automatically introduced from the diffusion pump. A phase-separated/ crystalline nanostructure (Figure 5b,d) was confirmed to be formed for the present $C_{60}:H_2Pc$ co-deposited film.

Figure 7 shows the current-voltage (J-V) characteristics of the cells in Figure 6b with co-deposited layer thicknesses, *X*, of 250, 600, 960 nm, and 1.2 µm, incorporating a C_{60} sample purified three times by single-crystal sublimation. Figure 8 shows the dependence of the fill-factor (FF) and the short-circuit photocurrent density (J_{sc}) on *X*. Surprisingly, FF hardly decreases even for an extremely thick *i*-codeposited layer of 1.2 µm (black open dots). Simultaneously, J_{sc} increases with *X* and reaches a maximum value of 19.1 $mAcm^{-2}$. On the contrary, when the C_{60} is purified by conventional train sublimation under vacuum, FF monotonically decreases with co-deposited layer thickness (Figure 3a, red open squares) [18]. At *X* = 960 nm, a J_{sc} value of 18.3 $mAcm^{-2}$ and a conversion efficiency of 5.3% were observed [19–21]. The internal quantum efficiency reaches around 90% in the region from 400 to 700 nm for the *X* = 960 nm cell (Figure 9a).

Figure 7. Current-voltage (J-V) characteristics for *p-i-n* cells with *i*-layer thicknesses (*X*) of 250 nm, 600 nm, 960 nm, and 1.2 µm. Cell parameters (*X* = 960 nm); J_{sc}: 18.3 $mAcm^{-2}$, V_{oc}: 0.40 V, FF: 0.53, Efficiency: 5.3%. The simulated light intensity transmitted through the ITO glass substrate is 74.2 $mWcm^{-2}$.
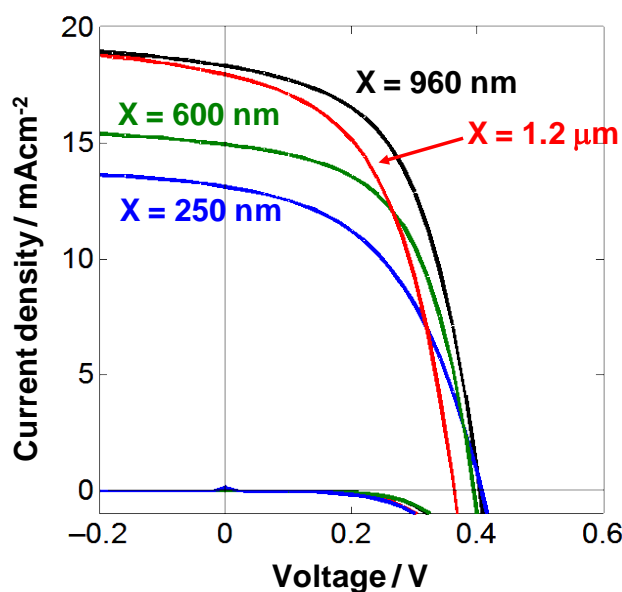
Figure 8. (**a**) Dependence of fill factor (FF) on the C_{60}:H_2Pc *i*-interlayer thickness (*X*) for *p-i-n* cells incorporating C_{60} purified three times by single-crystal formed sublimation (black open dots) and for *p-i-n* cells incorporating C_{60} purified by conventional train sublimation under vacuum (red open squares); (**b**) Dependence of short-circuit photocurrent density (J_{sc}) on *X*.

(**a**)　　　　　　　　　　(**b**)
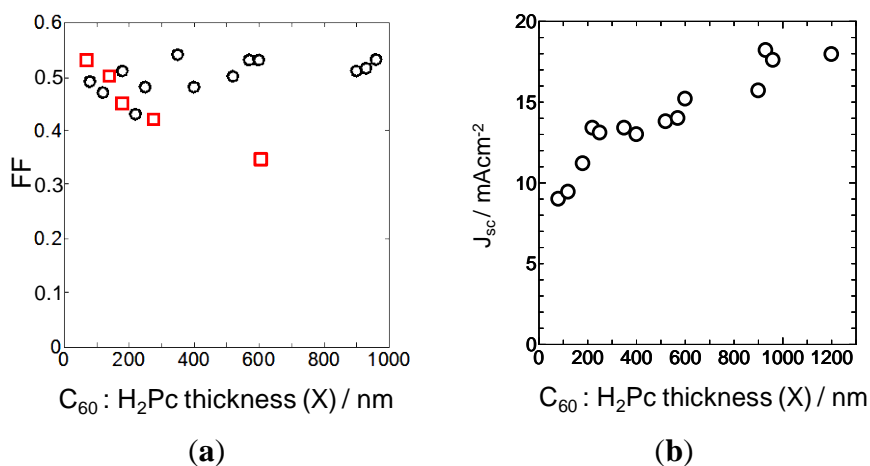
Figure 9. (**a**) Spectral dependence of the internal quantum efficiency for a cell with *X* = 960 nm; (**b**) Spectral dependences of the light absorption ratio of cells with *X* = 180 nm (curve A), 600 nm (curve B), and 960 nm (curve C); (**c**) Photograph of cells with *X* = 180 nm (top) and 960 nm (bottom).
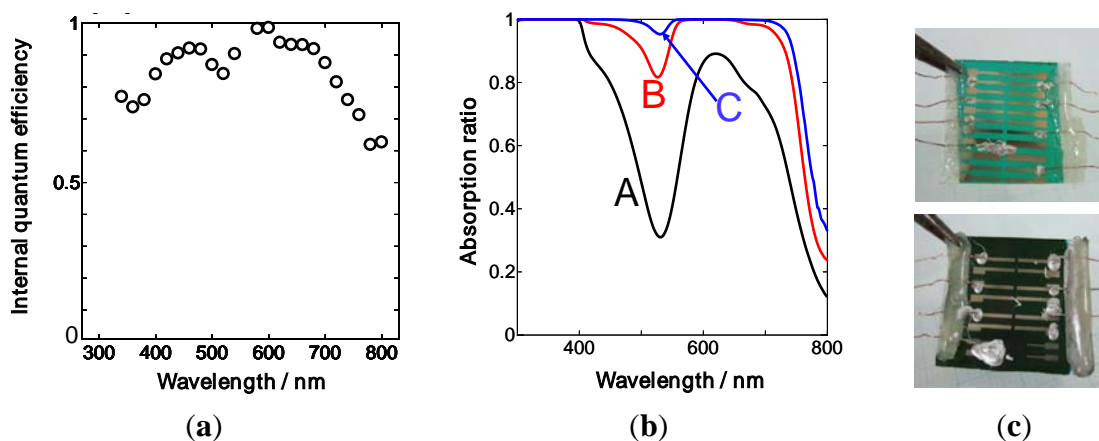

(**a**)　　　　　　　　(**b**)　　　　　　　　(**c**)

Figure 9b shows the spectral dependence of the absorption ratio of the cells. For a thin C_{60}:H_2Pc layer (*X* = 180 nm, curve A), a large portion of the visible light, especially around 500 nm, cannot be absorbed due to the low absorbance of C_{60}. For an extremely thick C_{60}:H_2Pc layer (*X* = 960 nm, curve C), 95% of the visible light from 300 to 800 nm is absorbed. Figure 9c shows photographs of the cells with *X* = 180 nm (top) and 960 nm (bottom). For *X* = 180 nm, the cell color is a transparent green, *i.e.*, a large portion of the visible light is not absorbed and therefore cannot be utilized. For *X* = 960 nm, the cell color is an opaque dark brown, *i.e.*, almost all of the visible light is absorbed. The most important feature of the present cells is the incorporation of an extremely thick (1 µm) C_{60}:H_2Pc co-deposited layer into the cell without decreasing FF. This allows the utilization of the entire visible region of solar light.

To evaluate the purity of the C_{60} crystals at the ppm level, secondary ion mass spectroscopy with a Cs^+ ion source (SIMS, ULVAC-PHI, 6650M) was used. Figure 10 shows the negative ion mass spectrum (a) and the depth profile (b). Most of the peaks are assigned to carbon (C_1, C_2, *etc.* and their isotopes). As impurities, only oxygen (O) and hydrogen (H) were detected. The intensity of 10^1 in the depth profile corresponds to the detection limit for the elements. For O atoms, the detection limit corresponds to a concentration of about 8×10^{15} atoms/cm^3 [22]. Taking this value into account, we conclude that the purity of the C_{60} has reached at least seven-nines (99.99999%, 7N) [23]. The main impurity is revealed to be oxygen. C_{60} molecules interacting with oxygen seem to be the main impurities. Oxidized C_{60} ($C_{60}O_x$) has been reported to act as an electron trap [24]. It is probable that the absence of $C_{60}O_x$ traps greatly enhances the electron diffusion length ($L = (D\tau)^{1/2}$; D: diffusion coefficient, τ: electron lifetime) by increasing the lifetime (τ).

Figure 10. Negative ion mass spectrum (**a**) and depth profile (**b**) of SIMS measurements for C_{60} crystal purified three times by single-crystal sublimation.
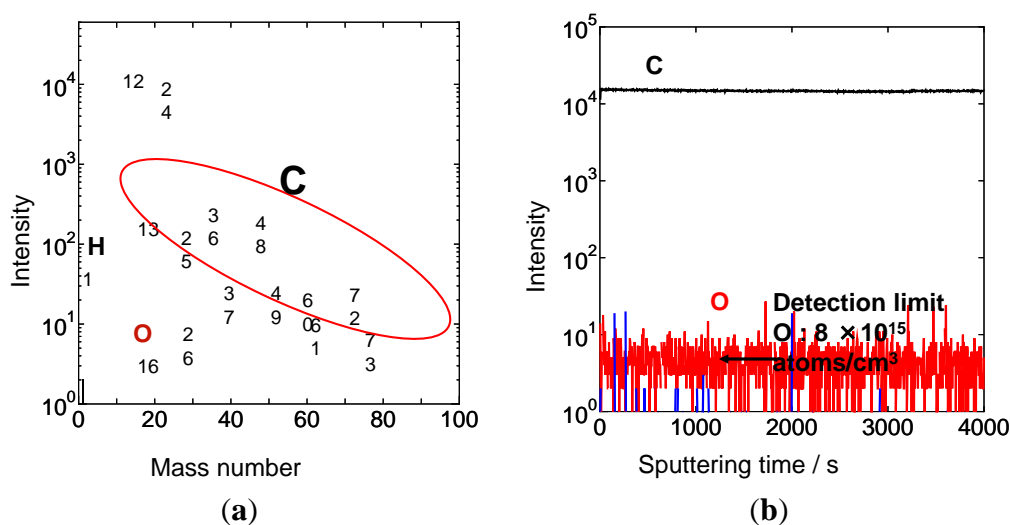
The overall results in this Section suggest that both high-purification and phase-separation are necessary to fabricate 1 µm-thick C_{60}:H_2Pc co-deposited cells.

5. *pn*-Control by Doping

5.1. Background

Organic semiconductors have been recognized as being affected by unintentional contamination from impurities that act as donors, acceptors, traps, *etc*. Uncontrolled impurities due to incomplete purification and due to contamination from air hid the real nature of organic semiconductors for a long time. A typical example is oxygen. Since oxygen from air, which acts as an acceptor impurity, is doped in many kinds of organic semiconductors such as phthalocyanines, they always show *p*-type character. The prevention of exposure to oxygen by the use of ultra-high vacuum during film deposition and subsequent measurements has revealed that phthalocyanines are fundamentally *n*-type in nature [25,26]. A few exceptional kinds of organic semiconductors, such as perylene pigments (for example Im-PTC (Figure 3)) that are not affected by oxygen even in air show *n*-type character.

Though impurity doping into organic semiconductors has already been studied, the types of dopants that were used were very limited. As acceptor dopants, halogen vapors, such as I_2 or Br_2, were used [27,28]. After Br_2-doping, perylene pigment changed its conduction type from *n*- to *p*-type, and *pn*-homojunctions could be formed [29]. On the other hand, as donor dopants, there were few choices except alkaline metals, such as Na and Ca, which are easily oxidized in air.

In the last decade, however, due to spin-offs from organic EL technology, several new kinds of dopants have been identified, firstly for the carrier injection layers. As acceptors, organic dopants such as F_4-TCNQ [30,31] and inorganic dopants like MoO_3, V_2O_5, *etc*. [32,33] were found. In terms of donors that are relatively stable in air, Harada *et al*. found a Ru-complex and applied it to fabricate *pn*-homojunctions in zinc phthalocyanine [34,35] and pentacene [36]. Recently, compounds of alkaline metals, such as Cs_2CO_3 [37,38], and Co-complexes [39] acting as donor dopants have been identified. Progress in the search for dopants for organic semiconductors is summarized in reference [40].

We believe that the following points are indispensable for the complete *pn*-control of organic semiconductors. (a) a ppm-level doping technique should be applied to sub-ppm purified organic semiconductors; (b) Complete *pn*-control, *i.e*., the observation that every single organic semiconductor shows both *n*- and *p*-type characteristics by impurity doping alone, should be proved; (c) Uncontrollable doping by oxygen and water from air should be completely avoided to obtain reproducible results; (d) For organic solar cell applications, the doping technique should be applicable not only to single organic semiconductor films, but also to co-deposited films that have D/A sensitization capability.

5.2. Method of ppm-Level Doping

Organic semiconductor samples of at least 7N purity were used. C_{60} (nano purple TL, Frontier Carbon, Tokyo, Japan), H_2Pc (Fastogen Blue EP-101, Dainippon Ink and Chemicals, Inc., Tokyo, Japan), and 6T (sexithiophene; Tokyo Chemical Industry, Tokyo, Japan) samples were purified by growing single-crystals by sublimation, as mentioned in Section 4.1. MoO_3 (Alfa Aeser, 99.9995%) and V_2O_5 (Aldrich, 99.99%), and Cs_2CO_3 (Aldrich, 99.995%) were used as dopants for acceptors and donors, respectively (Figure 11a).

Figure 11. (**a**) Three-sources co-deposition. MoO_3 and V_2O_5 acting as acceptors and Cs_2CO_3 acting as a donor were doped into the $H_2Pc:C_{60}$ (1:1) co-deposited film; (**b**) An example of the total-thickness signal from the QCM *vs*. time relationship for 9 ppm doping.

(**a**)   (**b**)
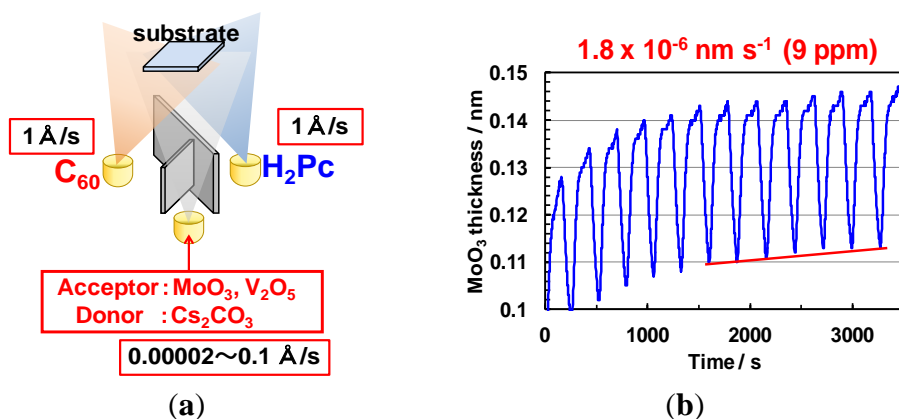
Multiple component co-evaporation techniques were employed to simultaneously evaporate organic semiconductors and dopants. In the case of doping into single organic semiconductor films, a two-component co-evaporation technique was employed. In the case of doping into C_{60}:H_2Pc and C_{60}:6T co-deposited films, a three-component co-evaporation technique (Figure 11a) was employed. An oil-free vacuum evaporator (ET300-6E-HK, EpiTech Inc., Kyoto, Japan) was used for co-evaporation on indium tin oxide (ITO) glass substrates at a chamber pressure of 10^{-5} Pa.

Precise monitoring of the deposition rate using a quartz crystal microbalance (QCM) equipped with a computer monitoring system (ULVAC, CRTM-6000G/Depoview) allowed us to introduce the dopants down to a very low concentration of 10 ppm by volume. Figure 11b shows an example of the total-thickness signal for the QCM *vs.* time relationship as monitored by a PC display for 50 ppm MoO_3 doping. There was a very slow cyclical fluctuation in the material due to temperature fluctuations in the cooling water for the QCM caused by on/off cycling of the chiller. However, a reproducible increase in the baseline (red line), which was only observed during MoO_3 evaporation for a prolonged timescale of 3500 s, was observed (1.8×10^{-6} nm s^{-1}). The evaporation rate of the organic semiconductors was maintained at 0.2 nm s^{-1}. Therefore, a doping concentration of 9 ppm in volume can be obtained ($1.8 \times 10^{-6}/0.2 = 9 \times 10^{-6}$).

The Fermi level (E_F) of the 100 nm-thick organic semiconductor films was measured using a Kelvin vibrating capacitor apparatus (Riken-Keiki, FAC-1). Both the evaporation chamber and the Kelvin probe were built into a glove-box (Miwa, DBO-1.5) purged with N_2 gas ($O_2 < 0.2$ ppm, $H_2O < 0.5$ ppm). During the film deposition and the E_F and photovoltaic measurements, none of the organic films were exposed to air at any time. Removal of the influence of O_2 is indispensable for obtaining accurate E_F measurements of organic semiconductor films. The E_F values were easily perturbed if the organic films were exposed to air even once, especially by the ingress of O_2 into the films, and then reproducible results could hardly be obtained.

## 5.3. pn-Control of Single C_{60} Films

In Figure 12, energy diagrams of the C_{60} (left side) and MoO_3 (right side) films are shown. The MoO_3 showed a remarkably positive value of E_F at 6.69 eV, which is more positive than the upper edge of the valence band of C_{60} (6.4 eV), as determined by X-ray photoelectron spectroscopy [41,42]. The value of E_F for non-doped C_{60} (black line) is located at 4.6 eV, near the lower edge of the conduction band, suggesting that this film is *n*-type in nature. When MoO_3 was doped at a concentration of 3000 ppm, the value of E_F shifted toward the positive direction and reached 5.88 eV, which is close to the upper edge of the valence band (6.4 eV). This result strongly suggests that MoO_3-doped C_{60} is *p*-type.

Figure 12. Energy diagrams of various organic semiconductor films. The black, red, and blue lines show the energetic position of E_F for non-doped, MoO_3-doped, and Cs_2CO_3-doped films. The doping concentration is 3000 ppm. E_F vales for MoO_3 and Cs_2CO_3 films (100 nm) are also shown.
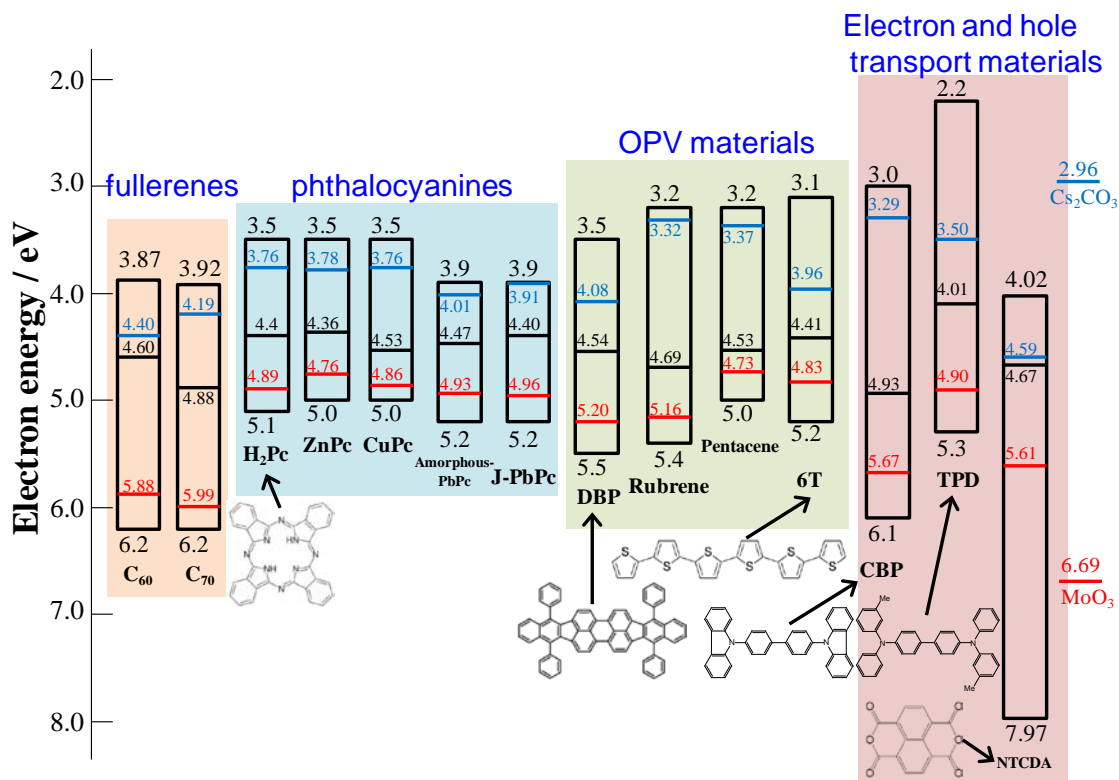
To investigate the kinds of interactions that occur between C_{60} and MoO_3, the absorption spectra of a co-deposited film with a ratio of 1:1 were obtained. Though single films of MoO_3 and C_{60} are transparent and weak-yellowish transparent respectively, a new strong absorption from 500 to 1800 nm appeared for the co-deposited MoO_3:C_{60} (1:1) film and the film color changed to black (Figure 13, left upper photograph). This new absorption can be attributed to charge transfer (CT) absorption between C_{60} and MoO_3. Absorption spectrum of CT band is appeared in reference [43]. Based on the energy diagram (Figure 12), it is reasonable to infer that MoO_3 extracts electrons from the valence band of C_{60}. The left-middle figure in Figure 13 shows the mechanism of p-type C_{60} formation. A CT complex, *i.e.*, $C_{60}^+ - MoO_3^-$, is formed. Here, the negative charge on the MoO_3^- group can be regarded as a spatially-fixed ion, *i.e.*, an ionized acceptor. On the other hand, the positive charge on C_{60}^+ can be liberated from the negative charge on the MoO_3^- by heat energy at room temperature, and can migrate into the C_{60} film and act as a free hole in the valence band of C_{60}. This increase in hole concentration causes the large positive shift of E_F that is observed (Figure 12). This is a process similar to the formation of free holes in p-type silicon (Figure 13, left lower). V_2O_5 was also confirmed to act as an acceptor in C_{60}.

Figure 13. (Upper) Photographs of C_{60}:MoO_3 (1:1) (left) and C_{60}:Cs_2CO_3 (10:1) (right). Strong CT-absorption was observed. (Middle) Mechanisms of *p*- and *n*-type C_{60} formation by MoO_3 (left) and Cs_2CO_3 (right) doping. (Lower) Corresponding mechanisms of *p*- and *n*-type Si formation by B (left) and P (right) doping.
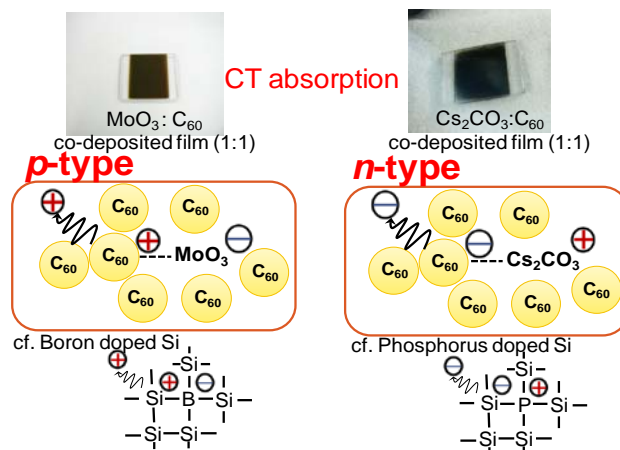

For the 3000 ppm Cs_2CO_3-doped C_{60} film, the value of E_F shifted negatively to 4.40 eV, which is close to the lower edge of the conduction band (CB) of C_{60} (4.0 eV) [41]. A thick co-deposited film of C_{60}:Cs_2CO_3 in the ratio 10:1 changed color to reddish-brown (Figure 13, right upper photograph), *i.e.*, it showed a new broad CT absorption. Since the work function of Cs_2CO_3 (2.96 eV) is more negative than the conduction band of C_{60} (4.0 eV), it is reasonable that Cs_2CO_3 donates an electron to C_{60} and forms a CT complex, *i.e.*, $C_{60}^- - Cs_2CO_3^+$. The formation of n-C_{60} by Cs_2CO_3 doping is caused by the opposite mechanism to MoO_3 doping (Figure 13). The donor ability of Cs_2CO_3 did not disappear even after exposure to air.

*5.4. pn-Homojunction Formation in Single C_{60} Films*

Since both *p*- and *n*-type C_{60} were formed, we tried to fabricate *pn*-homojunctions in the single C_{60} films [44,45]. Three types of cells with different thickness combinations of *p*- and *n*-doped layers, *i.e.*, 250/750 nm (a); 500/500 nm (b); and 750/250 nm (c) were fabricated (Figure 14). The total thickness of the C_{60} was maintained at 1 µm for all cells. Figure 15 shows the action spectra for the three types of cells. Under irradiation onto the ITO electrode (Figure 14a, hν(ITO)) and with the homojunction located at the ITO side (Figures 14a and 15a, curve A), photocurrent mainly appeared between 400 and 500 nm, which corresponds to the visible absorption region of the C_{60} film (black curve). For the homojunction at the center of the cell (Figures 14b and 15a, curve B), the photocurrent decreased and shifted to longer wavelength and the main peak was located at the edge of the C_{60} absorption. Finally, for the homojunction on the Ag side (Figures 14c and 15a, curve C), the low magnitude photcurrent shifted to a wavelength far longer than 500 nm, where there is little C_{60} absorption. The observed systematic change in the shape of the action spectra with respect to the distance of the homojunction from the light-irradiated electrode can be attributed to the so-called "masking effect". This means that photocarrier generation occurs mainly in the neighboring regions of the *p/n*-doped interface (active zone) and that, by retracting this homojunction from the light-irradiated ITO surface, a dead layer is gradually grown in front of this active zone.

Figure 14. Three structures of *pn*-homojunction C_{60} cells. The thickness combinations of the MoO_3- and Ca-doped layers are 250/750 nm (**a**); 500/500 nm (**b**); and 750/250 nm (**c**). The concentration was kept at 5000 ppm for both dopants. Hν (ITO) and hν (Ag) denote light irradiation onto the ITO and onto Ag electrodes, respectively. The locations of the homojunctions are indicated by the arrows.
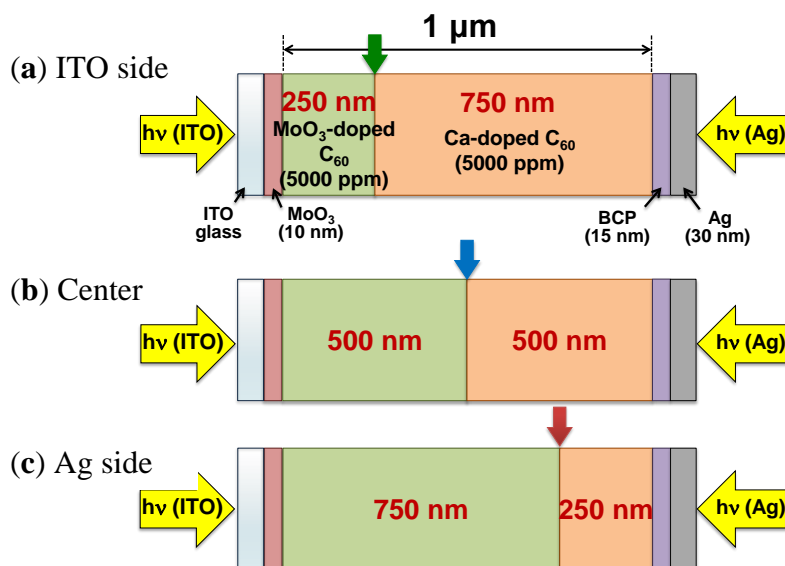
Figure 15. Action spectra of the short-circuit photocurrent density (J_{sc}) under irradiation onto the ITO electrode (**a**) (hν(ITO)) and onto the Ag electrode (**b**) (hν(Ag)). Curves A, B, and C are for cells (**a**); (**b**); and (**c**) in Figure 14, respectively. The black curve shows the absorption spectrum of the C_{60} film (150 nm). The monochromatic light intensity irradiated to the electrodes is around 3 mWcm^{-2}.
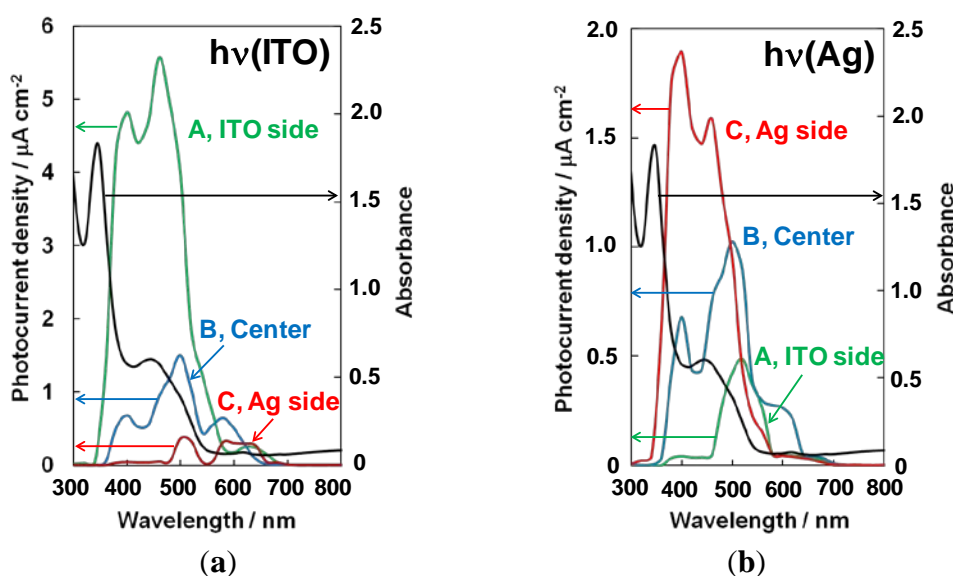

Under light irradiation onto the Ag electrode (Figure 14, hν(Ag)), the homojunction approaches the illuminated electrode in the order of cells (a); (b); and (c). In this case, completely the reverse tendency, namely, an increase in the magnitude of the photocurrent and a shift towards shorter wavelength of the action spectra, were observed (Figure 15b, curves C, B, and A). This means that the

dead layer between the active zone and the illuminated Ag electrode gradually disappeared. Apparently, the photoactive zone moves together with the homojunction. Even if the Ca donors were substituted with Cs_2CO_3 donors, fundamentally the same result was obtained. Since the width of the depletion layer *pn*-homojunction at the present doping concentrations of 5000 ppm MoO_3/5000 ppm Cs_2CO_3 is calculated to be only 29 nm, which is far smaller than the total cell thickness of 1 µm, a strong masking effect (Figure 15) was observed.

In Figure 16, the energy structure of a *pn*-homojunction (doping concentration: 3000 ppm MoO_3/500 ppm Cs_2CO_3) as measured by Kelvin-band mapping (see Sections 5.6 and 6.3) is shown. Since there is a significant difference in E_F, a built-in potential can be created by contacting the MoO_3- and the Cs_2CO_3-doped C_{60} films (Figure 12, left side). As a result, a *pn*-homojunction is formed. The observed direction of the photovoltage, whereby ITO/MoO_3 is positive and BCP/Ag is negative, is consistent with this energy structure. The present results clearly show that *pn*-homojunctions were fabricated in the single C_{60} films by doping alone. In other words, the photovoltaic properties of organic semiconductor films could be intentionally designed by doping. We also confirmed the formation of *pn*-homojunctions for metal-free phthalocyanine (H_2Pc) [46].

Figure 16. Energetic structure of *pn*-homojunction formed after contact measured by Kelvin band mapping. The doping concentrations of Cs_2CO_3 and MoO_3 are 500 ppm and 3000 ppm, respectively.
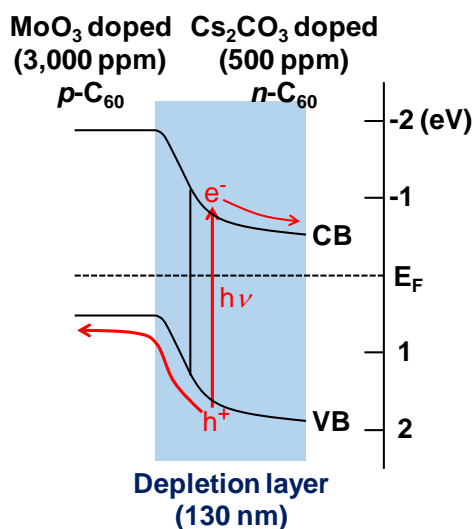
5.5. Generality

As shown in Figure 12, other than fullerenes (C_{60} and C_{70}), complete *pn*-control was accomplished for various phthalocyanines (H_2Pc, ZnPc CuPc, PbPc), other photovoltaic organic semiconductors (rubrene, sexithiophene (6T), pentacene, DBP), and hole transport materials (CBP). In exceptional cases, due to the energy relationship, only *p*- and *n*-type control could be accomplished for TPD and electron transport material (NTCDA), respectively. These results strongly suggest that, in principle, almost all single organic semiconductors can be controlled to both *n*-type and *p*-type by doping alone, similar to the case of inorganic semiconductors. For the cases of C_{60}, H_2Pc, ZnPc, pentacene, and CBP, *pn*-homojunctions were formed [34,36,38,44,46].

5.6. Band Mapping by Kelvin Probe

The concentrations of carriers created by doping can be evaluated by using the Kelvin vibrating capacitor method [47,48]. Figure 17 shows the principle of band mapping by Kelvin probe. When *p*-doped organic semiconductors are in contact with ITO electrodes, the E_F values are aligned. Accordingly, the vacuum level (E_{VAC}) is bent upward and the value of the work function, which is defined as the difference between E_{VAC} and E_F (red double arrows), changes with the thickness of the films. Thus, the band-bending can be directly mapped (Figure 17, lower) by measuring the work function using a Kelvin probe for changing thicknesses of doped films (Figure 17, middle). Since the band-bending gives the depletion layer width (W_{dep}) and the built-in potential (V_{bi}), the carrier concentration (N) can be obtained by using the following equation; $W_{dep} = (2\varepsilon\varepsilon_0 V_{bi}/eN)^{1/2}$. Here, ε, ε_0, and e are the relative dielectric constant, the dielectric constant of a vacuum, and the elementary charge.

Figure 17. Principle of band-mapping by Kelvin probe. An interface between an ITO and a *p*-type semiconductor film is shown. Work function values (middle figure) corresponding to the double red arrows (lower figure) depending on the thickness of the organic semiconductor film were measured by Kelvin probe. E_{vac}, E_F, CB, and VB denote the vacuum level, the Fermi level, the conduction band, and the valence band, respectively.
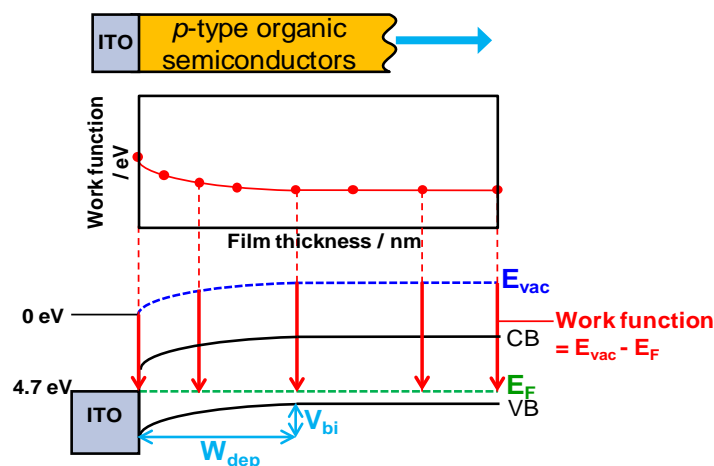

Figure 18 shows the dependences of the work functions of the doped C_{60} films on the film thicknesses. In the case of Cs_2CO_3-doping, the work function was shifted toward the negative direction and reached close to the lower edge of the conduction band (CB) (3.9 eV) (triangular dots). In the case of MoO_3-doping, the work function was shifted toward the positive direction and reached near the upper edge of the valence band (VB) (6.4 eV) (circular dots). For both dopants, as the doping concentration increased, the film thickness at which the shift in the work function finished became thinner, and the magnitude of the energy shift became larger. Namely, W_{dep} decreased and V_{bi} increased. These band-bendings can be fitted by quadratic curves (Figure 18, solid lines) based on the Poisson equation, and the values of W_{dep} and V_{bi} can be precisely determined. For example, in the cases of the *n*- and *p*-type band-bending of C_{60} films doped with Cs_2CO_3 (500 ppm) and with MoO_3 (5000 ppm), electron and hole concentrations of 2.5×10^{17} cm^{-3} and 9.6×10^{17} cm^{-3} [49] were obtained, respectively, from W_{dep} values of 24 nm and 21 nm and V_{bi} values of 0.29 V and 0.87 V using a ε value of 4.4 for C_{60} [50].

Figure 18. Work function shifts in C_{60} films doped with Cs_2CO_3 and MoO_3 on ITO substrates (triangular and circular dots). Band-bending was fitted by a quadratic relationship based on the Poisson equation (solid curves).
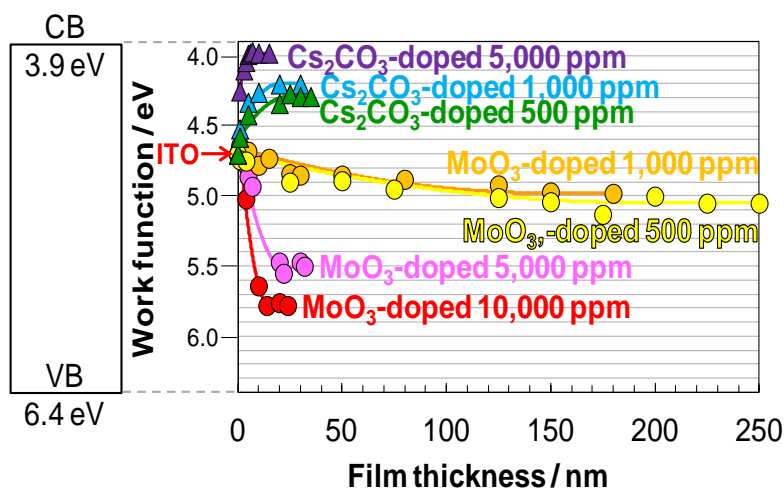

Figure 19a shows the dependence of carrier concentration on the doping concentration. When the Cs_2CO_3-doping concentration increased, the electron concentration rapidly increased and reached 10^{19} cm^{-3} at a doping concentration of 10,000 ppm. On the other hand, when MoO_3 was used as the dopant, the carrier concentration showed a minimum value, *i.e*., 4.3×10^{15} cm^{-3} at 500 ppm, and the hole concentration increased and reached 2.7×10^{18} cm^{-3} at 10,000 ppm. The minimum carrier concentration at 500 ppm with MoO_3-doping suggests that the holes created by MoO_3-doping compensate the inherent *n*-type nature of C_{60}.

Figure 19. Dependence of carrier concentration (**a**) and doping efficiency (**b**) on doping concentration of Cs_2CO_3 or MoO_3.
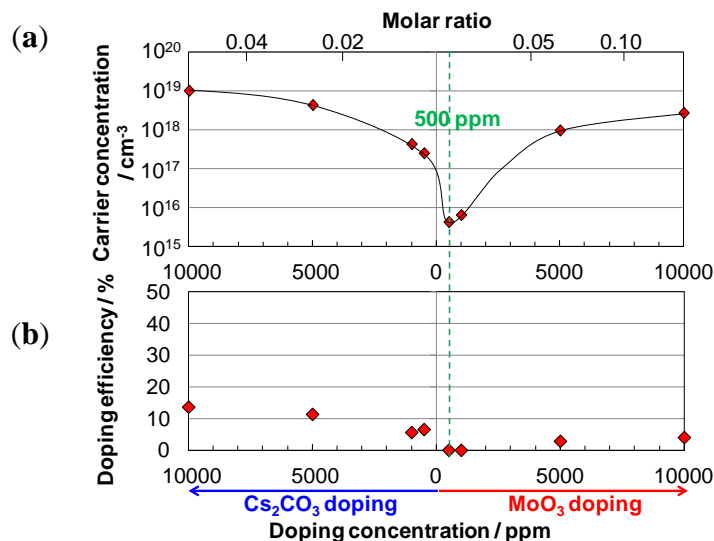

Figure 19b shows the doping efficiency, which is defined as the ratio of the induced carrier concentration to the doped molecular concentration. The doping efficiencies of Cs_2CO_3- and MoO_3-doping are about 10% and 3%, respectively. The doping process can be explained by the formation of a CT-complex and its subsequent ionization (Figures 13(middle) and 20b). Thus, the

doping efficiency is expressed by the product of the rates of CT complex formation and ionization. In the case of Cs_2CO_3, since Cs_2CO_3 is a substantial molecule, by assuming that Cs_2CO_3 evaporates molecularly and the rate of CT complex formation with C_{60} is close to unity [51], the observed doping efficiency of 10% can be regarded as the ionization efficiency, which is significantly smaller than the value of 100% obtained for the donor dopant P in Si at room temperature. The orbitals of the electrons around the positive charge on the ionized donor in the cases of P-doping in Si (a) and of Cs_2CO_3-doping in C_{60} (b) are shown in Figure 20. Based on the fact that the ε value of Si is 11.9, the radius of the orbital of the electron around the positive charge of an ionized donor (P^+) is calculated to be 3.3 nm. This situation is fundamentally the same to the Wannier exciton (Figure 1a) and the electron is easily liberated from the positive charge by thermal energy at room temperature, and thus the ionization efficiency reaches unity (Figure 20a). The only difference to the exciton is that the positive charge is spatially fixed in the crystal lattice [52]. In the case of Cs_2CO_3-doping in C_{60}, since the ε value of C_{60} is 4.4, the electron experiences a stronger attractive force from the positive charge. The radius of the Frenkel exciton is only 0.5 nm for C_{60} (Figure 1b). However, a CT complex is formed by employing Cs_2CO_3-doping, *i.e.*, $[Cs_2CO_3^+ - C_{60}^-]$ and the charges are separated on the neighboring molecules (Figure 20b). This situation is fundamentally the same as the CT exciton (Figure 2b) and the negative charge on C_{60} can be liberated by thermal energy at room temperature. Thus, significant values for the ionization efficiencies of electrons of about 10% were observed, though they were lower than the case of Si.

Figure 20. Orbital of an electron around a positive charge on an ionized donor. (**a**) P-doping in Si. P^+ is represented by the red shaded circle. This situation resembles the Wannier exciton (Figure 1a); (**b**) Cs_2CO_3-doping in C_{60}. $Cs_2CO_3^+$ is represented by the red shaded circle. This situation resembles the CT-exciton (Figure 2b).

(**a**)   (**b**)
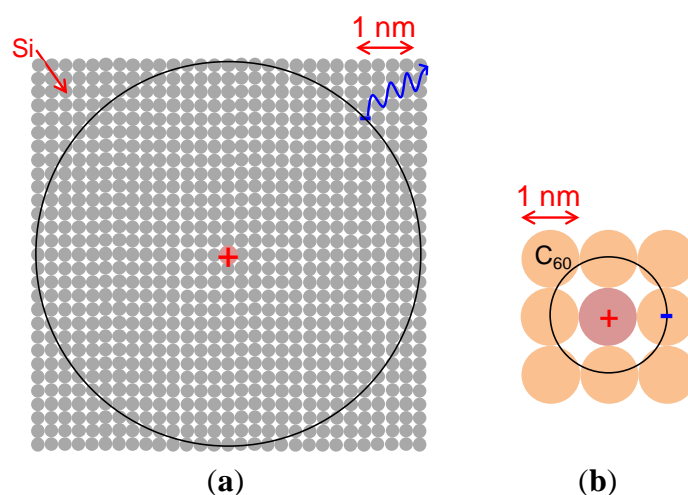
In the case of MoO_3, a doping efficiency of 3% was obtained under the assumption that MoO_3 forms the trimer (Mo_3O_9) [53]. Though a similar mechanism to that in Figure 20b can also be applied in this case, in addition, the formation of larger MoO_x clusters lowers the efficiency of CT-complex formation, which seems to lower the total doping efficiency.

5.7. Organic/Metal Ohmic Junction

It is very important to make the two organic/metal contacts in a photovoltaic cell ohmic. When the region in the vicinity of a metal electrode is heavily doped, even if there is a Schottky barrier, its width becomes extremely thin allowing charge carrier tunneling and, as a result, an ohmic contact is expected to be formed similar to that on heavily p^+- or n^+-doped inorganic semiconductors [40,54,55]. Here, + means heavily doped. Moreover, an ohmic contact can be formed irrespective of which electrode material is used, since tunneling is less dependent on the metal work function, enabling the cell structure to be inverted. This technique would allow flexibility in the design of the cell structure.

Figure 21. Structures of invertible two-layered H_2Pc/C_{60} cells with heavily-doped organic/metal interfaces. For the cells in (**a**,**b**), photogenerated holes and electrons are extracted to ITO and Ag, and to Ag and ITO, respectively. The total thicknesses of the H_2Pc and C_{60} films are kept the same; (**c**,**d**) Current-voltage (J-V) characteristics for the cell (**a**,**b**) (red curves). The blue curves are for cells without heavily doped interfaces. The photocurrent and the dark current are shown by the solid and broken curves, respectively. The ITO electrode was irradiated with simulated solar light (AM1.5, 100 mWcm^{-2}). Cell performances: (**a**) J_{sc}: 3.38 mAcm^{-2}, V_{oc}: 0.46 V, FF: 0.59, Efficiency: 0.91%; (**b**) J_{sc}: 2.70 mAcm^{-2}, V_{oc}: 0.43 V, FF: 0.49, Efficiency: 0.57%. Copyright$^{©}$ 2012 The Japan Society of Applied Physics.
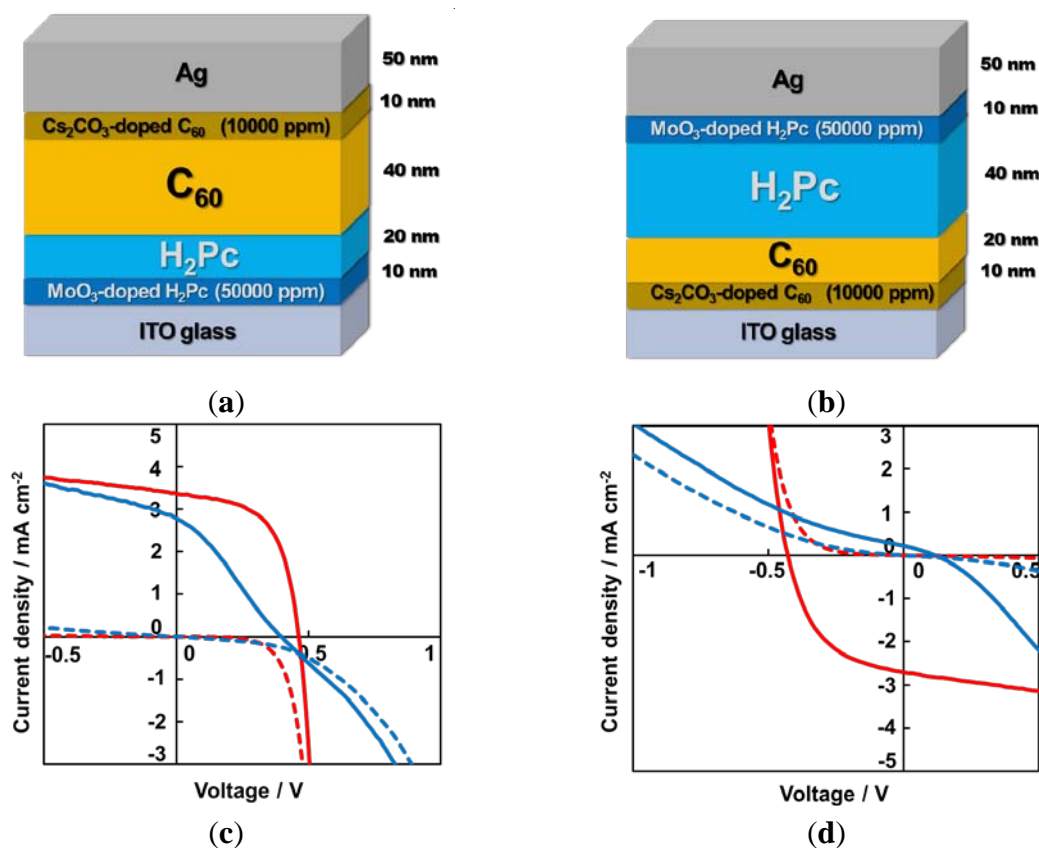

As a test case, two-layer cells consisting of C_{60} and H_2Pc (Figure 21a,b) were examined [56]. The electrode materials were ITO and Ag. Heavy doping of the order of 10,000 ppm (1%) and 50,000 ppm

(5%) was applied to thin 10 nm regions close to the C_{60} and H_2Pc/metal interfaces. Figure 21c,d shows the current-voltage (J-V) characteristics for the cells with heavily-doped regions in Figure 21a,b (red curves). For the cell in Figure 21a, the fill factor (FF) reaches a value of 0.59 and clear rectification characteristics can be seen with heavily-doped regions (red broken curve). Without the heavily-doped regions (blue curves), however, FF is only 0.29 and the forward current is significantly suppressed. For the inverted cell (Figure 21b), without heavily-doped regions (Figure 21d, blue curves), photovoltaic and rectification behavior are scarcely perceptible [57]. However, with the heavily-doped regions (red curves), the FF recovers, reaching a value of 0.49, and rectification is clearly observed. Clearly, the photovoltaic properties of the cells with thin heavily-doped regions at the interfaces are independent of the type of electrode material used. Thus, H_2Pc/C_{60} cells are invertible using this interfacial heavy-doping technique.

Since electron extraction from C_{60} to the ITO electrode is crucial for the operation of the inverted cell (Figure 21d (red curves)), we estimated the interfacial energy band structure of ITO/10,000 ppm Cs_2CO_3-doped C_{60} by Kelvin band mapping (Figure 22) (Section 5.6). There is a distinct barrier to electrons with a height of 0.34 eV from the conduction band of C_{60} to the ITO. However, since the band bends down steeply within 5 nm of the interface, photogenerated electrons can tunnel through this barrier. Heavily-doped C_{60} acts as an n^+-type semiconductor and makes the n^+-C_{60}/ITO junction ohmic. Organic/metal ohmic junctions can be fabricated by making tunneling contacts with heavy interfacial doping.

Figure 22. Energy structure for an ITO/n^+-C_{60} contact measured by Kelvin band mapping. A tunneling junction for photogenerated electrons is formed. Copyright© 2012 The Japan Society of Applied Physics.
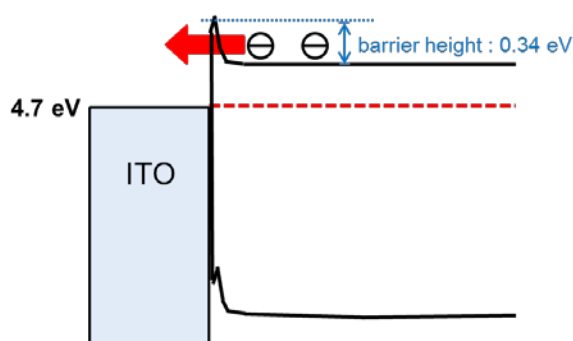
6. *pn*-Control of Co-deposited Films by Doping

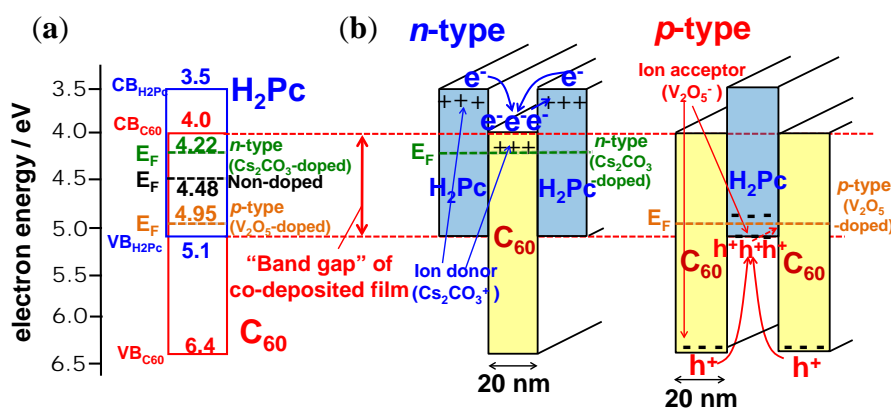### 6.1. pn-Control of Co-deposited Films

Co-deposited films consisting of D/A organic semiconductors are essential in order to generate photocurrent densities of significant magnitude based on the dissociation of excitons by the photoinduced electron transfer process (Figures 2b and 4). So, for the application of this doping technique to organic photovoltaic cells, doping should be performed by regarding a co-deposited film consisting two kinds of D/A organic semiconductors as a single semiconductor. We believe that the formation of a built-in potential by direct-doping in the bulk of co-deposited films, where the generation and transport of photocarriers occurs, has the potential to enhance the efficiency of these

cells [48]. Moreover, in these types of cells, short exciton diffusion length is no longer a factor that limits cell performance.

Figure 23a shows the energy diagram for $H_2Pc:C_{60}$ co-deposited films. With donor (Cs_2CO_3) doping, E_F has shifted from the undoped value of 4.48 eV (black broken line) to 4.22 eV (green broken line) and is close to the C_{60} conduction band (CB_{C60}). Conversely, for acceptor (V_2O_5) doping, E_F has shifted to 4.95 eV (orange broken line) and is close to the H_2Pc valence band (VB_{H2Pc}). Clearly, the conduction properties of the co-deposited films are controlled to both *n*- and *p*-type. It should be noted that the E_F shift occurs within the band gap of co-deposited H_2Pc and C_{60} films, *i.e.*, in between CB_{C60} and VB_{H2Pc}. For *n*-type doping (Figure 23b), free carriers (electrons) are produced in both H_2Pc and C_{60}, and they relax to the conduction band of C_{60}. E_F is fixed to 4.22 eV and is constant throughout the H_2Pc and C_{60} (green broken line). For *p*-type doping (Figure 23b), holes are produced that relax to the top of the H_2Pc valence band. E_F is fixed to 4.95 eV and is constant throughout the H_2Pc and C_{60} (orange broken line). As a result, the shifts in E_F are within the "bandgap of the co-deposited film". Thus, control of the doping in the co-deposited film was accomplished [58,59].

Figure 23. (**a**) *pn*-control of $H_2Pc:C_{60}$ co-deposited films by doping. The E_F shift occurs within the "bandgap of the co-deposited film". (**b**) Mechanism of *n*- and *p*-type formation.

6.2. Organic/Organic Ohmic Junction

pn-control technique of co-deposited films allows us to fabricate *pn*-homojunction in the uniform co-deposited films. Lightly doped *pn*-homojunction is expected to act as the photovoltaic cells. On the other hand, heavily doped n^+p^+-homojunction is expected to act as the organic/organic ohmic junction. In this section, behavior of heavily doped n^+p^+-homojunction is mentioned.

Irrespective of whether we use single or co-deposited films, by making an n^+p^+ heavily doped double layer, organic/organic ohmic junctions can be fabricated [45,60]. Figure 24a shows an n^+p^+-homojunction device fabricated in a $C_{60}:6T$ co-deposited film. MoO_3 and Cs_2CO_3 were heavily doped (50,000 ppm (5%)) for the p^+ and n^+-regions, respectively. Obviously, the n^+p^+-homojunction showed good ohmic properties (Figure 24b).

Figure 24. Organic/organic ohmic n^+p^+-homojunction (**a**) and its current-voltage characteristics (**b**).

(**a**)   (**b**)
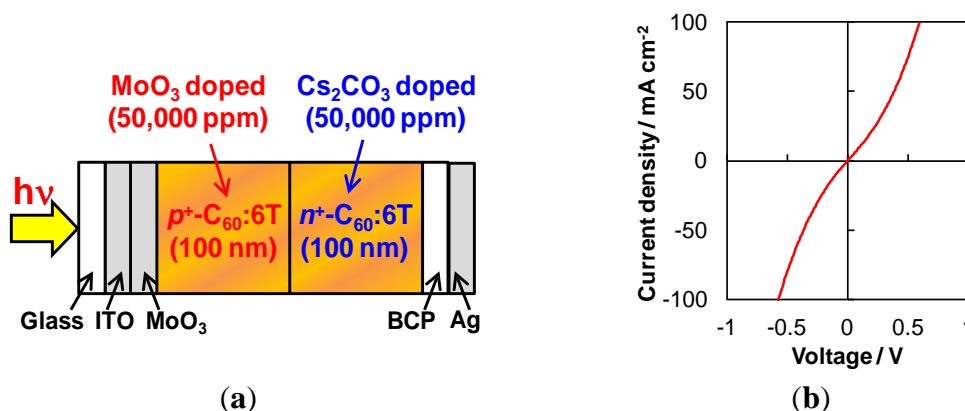
### 6.3. Tandem Cells Formed in Co-Deposited Films by Doping

Tandem organic solar cells were first reported by the authors in 1990 [61] and many types of cells that connect two unit cells have been fabricated [62]. The tandem organic solar cell, in which two single p^+in^+-homojunctions are connected by a heavily-doped n^+p^+-ohmic interlayer, were formed in co-deposited films consisting of C_{60} and sexithiophene (6T) simply by doping [60]. Figure 25a,b show the structures of a single p^+in^+-homojunction cell and a tandem cell connecting two p^+in^+-homojunctions formed in co-deposited C_{60}:6T films. The following cell parameters were obtained; J_{sc} of 3.0 mA cm^{-2}, V_{oc} of 1.69 V, FF of 0.47, and a conversion efficiency of 2.4% (Figure 25c, red curves B). Compared with the single cell (Figure 25c, blue curves A), V_{oc} has doubled from 0.85 V to 1.69 V. Obviously, the n^+p^+-homojunction in the tandem cell acts as an ohmic interlayer to connect the unit cells as shown in Figure 24.

Figure 25. (**a**) Structure of a p^+in^+-homojunction cell fabricated in a C_{60}:6T co-deposited film. A non-doped intrinsic C_{60}:6T layer is sandwiched between heavily doped p^+ and n^+-C_{60}:6T layers; (**b**) Structure of a tandem cell connecting two unit p^+in^+-homojunction cells via an ohmic n^+p^+-homojunction; (**c**) Current voltage (J-V) characteristics for a single p^+in^+-homojunction cell (blue curves A) and a tandem cell (red curves B). The photo and dark currents are shown by the solid and the broken curves, respectively. The ITO electrode was irradiated with simulated solar light (AM 1.5, 100 mW cm^{-2}). The cell parameters, *i.e.*, J_{sc}, V_{oc}, FF, and efficiency. Curve A: 4.5 mA cm^{-2}, 0.85 V, 0.41, 1.6%. Curve B: 3.0 mA cm^{-2}, 1.69 V, 0.47, 2.4%.
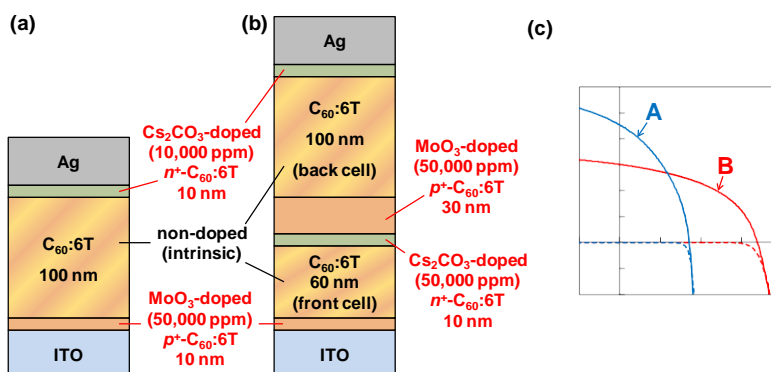
Kelvin energy-band mapping of the homojunctions was performed by measuring from both sides of the homojunction. To illustrate the presence of a p^+in^+-homojunction, the E_F values for non-doped C_{60}:6T films on doped films were measured (blue curves A in Figure 26a,b). E_F hardly changed and maintained almost constant values on both the MoO$_3$-doped film (Figure 26a) and on the Cs$_2$CO$_3$-doped (Figure 26b). These constant E_F values indicate that the non-doped C_{60}:6T films act as insulators. As a result, when a unit cell having the structure of MoO$_3$-doped (50,000 ppm)/non-doped/Cs$_2$CO$_3$-doped (50,000 ppm), *i.e.*, a p^+/insulator/n^+, is fabricated, the built-in electric field generated by the differences in E_F between the MoO$_3$ and Cs$_2$CO$_3$ doped layers (5.6 − 4.4 = 1.2 eV) (see Figure 26a,b), C_{60}:6T thickness = 0 nm) are uniformly distributed across the insulating non-doped C_{60}:6T film. Thus, two p^+in^+-homojunctions can be depicted in the front and back cells (Figure 27).

Figure 26. Energy level mapping of homojunctions using a Kelvin probe. The sample structures and the dependence of the position of the Fermi level (E_F) on the thicknesses of the non-doped or doped C_{60}:6T films are shown. (**a**) Non-doped (blue curve A) or Cs$_2$CO$_3$-doped (red curve B) deposited on a MoO$_3$-doped C_{60}:6T film; (**b**) Non-doped (blue curve A) or MoO$_3$-doped (red curve B) C_{60}:6T film deposited on a Cs$_2$CO$_3$-doped C_{60}:6T film.
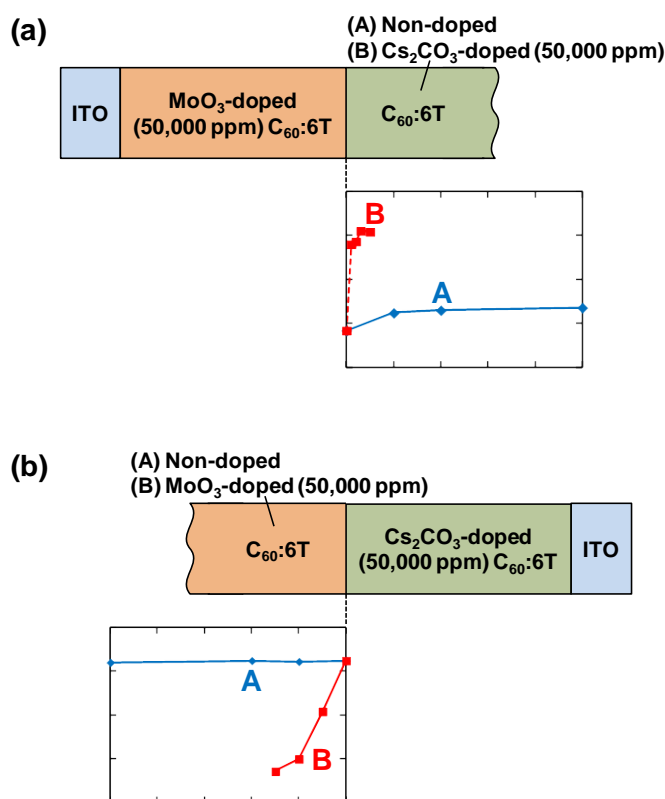
To illustrate the presence of an n^+p^+-homojunction, E_F values for Cs$_2$CO$_3$-doped films on MoO$_3$-doped films (red curve B in Figure 26a) and those for MoO$_3$-doped films on Cs$_2$CO$_3$-doped films (red curve B in Figure 26b) were measured. All doping concentrations of MoO$_3$ and Cs$_2$CO$_3$ are 50,000 ppm. In the former case, a rapid negative shift in E$_F$ ended within 3 nm and reached the original E_F position of Cs$_2$CO$_3$-doped C_{60}:6T (4.38 eV, see Figure 26b, C_{60}:6T thickness = 0 nm). In the latter case, a quick

positive shift in E_F ended within 15 nm and reached the original E_F position of MoO$_3$-doped C$_{60}$:6T (5.58 eV, see Figure 26a, C$_{60}$:6T thickness = 0 nm). Based on these complementary observations, the potential profile of the depletion layer of an n^+p^+-homojunction (Figure 27, red shaded region, width: 18 nm) can be drawn.

Figure 27. Energy band diagram of the depicted tandem cell based on Kelvin probe measurements (Figure 26). The red shaded region corresponds to the depletion layer for an n^+p^+-homojunction acting as an ohmic interlayer. VB and CB denote the valence band and the conduction band, respectively. The bands for C$_{60}$ and 6T are shown by the black and orange curves, respectively.
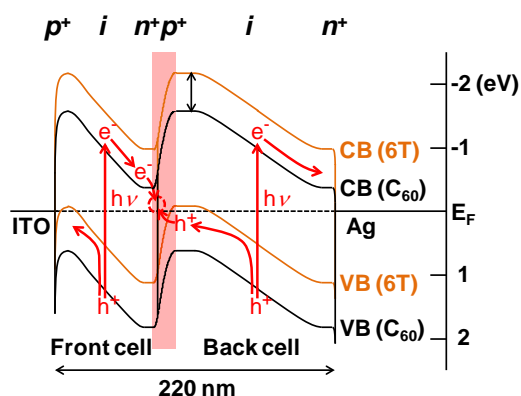
The overall energy band diagram of a tandem cell is shown in Figure 27. In the case of the p^+in^+-homojunction cells formed in co-deposited C$_{60}$:6T films, there are C$_{60}$/6T hetero interfaces where photoinduced electron transfer can occur throughout the whole of the cells. Thus, under light irradiation, electrons and holes are photo-generated in both the front and back cells. Electrons and holes that move toward the n^+p^+-ohmic interlayer neutralize each other due to recombination or tunneling. This process is consistent with the observed photovoltaic properties of the present tandem cell (Figure 25). It should be stressed that the present results proved that built-in potentials, like homojunctions and tandem junctions, can be intentionally formed in bulk co-deposited films induced by doping alone.

7. Conclusions

Factors that determine bandgap science for organic semiconductor films, namely, high-purification, *pn*-control by doping, built-in potential design, and precise evaluation of doping parameters, have been established. 7N-purification together with phase-separation by co-evaporant 3rd molecules allowed us to fabricate organic solar cells incorporating 1 µm-thick co-deposited films. *pn*-control techniques by impurity doping for both single and co-deposited films were established. A series of fundamental junctions, such as Schottky junctions, *pn*-homojunctions, p^+, n^+-organic/metal ohmic junctions, n^+-organic/p^+-organic ohmic homojunctions, and tandem cells were formed in single and co-deposited organic semiconductor films by doping alone.

Since conductivity (σ) is the product of the mobility (μ) and the carrier concentration (N), *i.e.*, $\sigma = eN\mu$ [e; electron charge], the cell resistance (σ^{-1}) can be reduced by increasing both N, by means

of doping, and μ, by means of phase-separation of the co-deposited film by using a co-evaporant 3rd molecule, Now, we are trying to combine doping with phase-separation [58].

Acknowledgments

Conflicts of Interest

The authors declare no conflict of interest.

References and Notes

1. *Organic Photovoltaics, Mechanisms, Materials and Devices*; Sun, S.-S., Sariciftci, N.S., Eds.; CRC Press: New York, NY, USA, 2005.
2. Spanggaard, H.; Krebs, F.C. A brief history of the development of organic and polymeric photovoltaics. *Sol. Energy Mater. Sol. Cells* **2004**, *83*, 125–146.
3. Hoppe, H.; Sariciftci, N.S. Organic solar cells: An overview. *J. Mater. Res.* **2004**, *19*, 1924–1945.
4. Tang, C.W. Two-layer organic photovoltaic cell. *Appl. Phys. Lett.* **1986**, *48*, 183–185.
5. Hiramoto, M.; Fujiwara, H.; Yokoyama, M. Three-layered organic solar cell with a photoactive interlayer of codeposited pigments. *Appl. Phys. Lett.* **1991**, *58*, 1062–1064.
6. Hiramoto, M.; Fujiwara, H.; Yokoyama, M. p-i-n like behavior in three-layered organic solar cells having a co-deposited interlayer of pigments. *J. Appl. Phys.* **1992**, *72*, 3781–3787.
7. Yu, G.; Gao, J.; Hummelen, J.C.; Wudl, F.; Heeger, A.J. Polymer photovoltaic cells: Enhanced efficiencies via a network if internal donor-acceptor heterojunctions. *Science* **1995**, *270*, 1789–1791.
8. Note: Precisely, since the exciton, *i.e.*, the bound electron-hole pair, resembles the hydrogen atom, quantized description is needed. Rydberg levels based on the Bohr's model of hydrogen atom can be expressed by the following equation; $E = E_G – G/n^2$ ($n = 1, 2, …$). (E_G: Ionization energy of the molecule in the solid. G: The exciton binding energy.) The exciton binding energy (G) is proportional to μ/mε. (μ: Reduced mass of exciton. m: Mass of electron. ε: Relative permittivity.) Thus, the exciton binding energy becomes large in the organic semiconductor having small value of ε.
9. Note: Exciton radius can be calculated based on the equation expressing the Bohr radius (r) including the relative permittivity (ε) and the reduced mass (m^*) between the effective mass of an electron (m_n^*) and a hole (m_p^*), *i.e.*, $r = \varepsilon_0 \varepsilon h^2/\pi m^* e^2$. Values of m^* are 0.14 and 0.94 for Si and C_{60}, respectively.
10. Peumans, P.; Yakimov, A.; Forrest, S.R. Small molecular weight organic thin-film photodetectors and solar cells. *J. Appl. Phys.* **2003**, *93*, 3693–3723.
11. Hiramoto, M.; Yamaga, T.; Danno, M.; Suemori, K.; Matsumura, Y.; Yokoyama, M. Design of nanostructure for photoelectric conversion using an organic vertical superlattice. *Appl. Phys. Lett.* **2006**, *88*, 213105.
12. Kaji, T.; Zhang, M.; Nakao, S.; Iketaki, K.; Yokoyama, K.; Tang, C.W.; Hiramoto, M. Co-evaporant induced crystalline donor:acceptor blends in organic solar cells. *Adv. Mat.* **2011**, *23*, 3320–3325.

13. Matsuo, Y.; Sato, Y.; Niinomi, T.; Soga, I.; Tanaka, H.; Nakamura, E. Columnar structure in bulk heterojunction in solution-processable three-layered *p-i-n* organic photovoltaic devices using tetrabenzoporphyrin precursor and silylmethyl[60]fullerene. *J. Am. Chem. Soc*. **2009**, *131*, 16048–16050.

14. Wagner, H.J.; Loutfy R.O.; Hsiao, C. Purification and characterization of phthalocyanines. *J. Mater. Sci*. **1982**, *17*, 2781–2791.

15. Laudise, R.A.; Kloc, Ch.; Simpkins, P.G.; Siegrist, T. Physical vapor growth of organic semiconductors. *J. Cryst. Growth* **1998**, *187*, 449–454.

16. Suemori, K.; Miyata, T.; Yokoyama, M.; Hiramoto, M. Organic solar cells protected by very thick naphthalene tetracarboxylic anhydride films. *Appl. Phys. Lett*. **2004**, *85*, 6269–6271.

17. Surmori, K.; Yokoyama, M.; Hiramoto, M. Electrical shorting of organic photovoltaic films resulting from metal migration. *J. Appl. Phys*. **2006**, *99*, 036109.

18. Suemori, K.; Miyata, T.; Yokoyama, M.; Hiramoto, M.; Three-layered organic solar cells incorporating nanostructure-optimized Phthalocyanine:Fullerene codeposited interlayer. *Appl. Phys. Lett*. **2005**, *86*, 063509.

19. Sakai, K.; Hiramoto, M. Efficient organic p-i-n solar cells having very thick codeposited i-layer consisting of highly purified organic semiconductors. *Mol. Cryst. Liq. Cryst*. **2008**, *491*, 284–289.

20. Hiramoto, M. Efficient organic p-i-n solar cells having very thick codeposited i-layer composed of highly purified organic semiconductors. *Proc. SPIE* **2008**, *7052*, doi:10.1117/12.798120.

21. Note: Thick NTCDA protection against electrical shorting is no longer needed since the *i*-layer has sufficient thickness. So, we could replace NTCDA (600 nm) with C_{60} (80 nm)/bathocuproine (BCP; 15 nm) or C_{60} (80 nm)/NTCDA (80 nm)/bathocuproine (BCP; 15 nm) and obtain similar results. For the latter case, cell parameters are J_{sc}: 17.5 mAcm^{-2}, V_{oc}: 0.44 V, FF: 0.57, efficiency: 5.3% (81.8 mWcm^{-2}).

22. Brenninghoven, A.; Rundenauer, F.G.; Werner, H.W. *Secondary Ion Mass Spectrometry*; John Wiley & Sons: New York, NY, USA, 1987.

23. Note: Purity of 7N was also confirmed by temperature programmed desorption mass spectroscopy.

24. Tanaka, Y.; Kanai, K.; Ouchi, Y.; Seki, K. Oxygen effect on the interfacial electronic structure of C_{60} film studied by ultraviolet photoelectron spectroscopy. *Chem. Phys. Lett*. **2007**, *441*, 63–67.

25. Martin, M.; Andre, J.-J.; Simon, J. Influence of dioxygen on the junction properties of metallophthalocyanine based devices. *J. Appl. Phys*. **1983**, *54*, 2792–2794.

26. Tada, H.; Touda, H.; Takada, M.; Matsushige, K. Quasi-intrinsic semiconducting state of titanyl-phthalocyanine films obtained under ultrahigh vacuum conditions. *Appl. Phys. Lett*. **2000**, *76*, 873–875.

27. Akamatsu, H.; Inokuchi, H.; Matsunaga, Y. Electrical conductivity of the perylene-bromine complex. *Nature* **1954**, *173*, 168–169.

28. Hiramoto, M.; Ihara, K.; Fukusumi, H.; Yokoyama, M. Conduction type control from n- to p-type for organic pigment film purified by reactive sublimation. *J. Appl. Phys*. **1995**, *78*, 7153–7157.

29. Hiramoto, M.; Ihara, K.; Yokoyama, M. Fermi level shift in photoconductive organic pigment films measured by Kelvin vibrating capacitor method. *Jpn. J. Appl. Phys*. **1995**, *34*, 3803–3807.

30. Huang, J.S.; Pfeiffer, M.; Werner, A.; Blochwitz, J., Leo, K.; Liu, S.Y. Low-voltage organic electroluminescent devices using pin structures. *Appl. Phys. Lett*. **2002**, *80*, 139–141.

31. Blochwitz, J.; Pfeiffer, M.; Fritz, T.; Leo, K. Low voltage organic light emitting diodes featuring doped phthalocyanine as hole transport material. *Appl. Phys. Lett.* **1998**, *73*, 729–731.

32. Tokito, S.; Noda, K.; Taga, Y. Metal oxides as a hole-injecting layer for an organic electroluminescent device. *J. Phys. D* **1996**, *29*, 2750–2753.

33. Matsushima, T.; Kinoshita, Y.; Murata, H. Formation of Ohmic hole injection by inserting an ultrathin layer of molybdenum trioxide between indium tin oxide and organic hole-transporting layers. *Appl. Phys. Lett.* **2007**, *91*, 253504:1–253504:3.

34. Harada, K.; Werner, A.G.; Pfeiffer, M.; Bloom, C.J.; Elliott, C.M.; Leo, K. Organic homojunction diodes with a high built-in potential: interpretation of the current-voltage characteristics by a generalized einstein relation. *Phys. Rev. Lett.* **2005**, *94*, 036601:1–036601:4.

35. Chan, C.K.; Zhao, W.; Barlow, S.; Marder, S.; Kahn, A. Decamethylcobaltocene as an efficient *n*-dopant in organic electronic materials and devices. *Org. Electron.* **2008**, *9*, 575–581.

36. Harada, K.; Riede, M.; Leo, K. Pentacene homojunctions: Electron and hole transport properties and related photovoltaic responses. *Phys. Rev. B* **2008**, *77*, 195212:1–195212:9.

37. Liao, H.-H.; Chen, L.-M.; Xu, Z.; Li, G.; Yang, Y. Highly efficient inverted polymer solar cell by low temperature annealing of Cs_2CO_3 interlayer. *Appl. Phys. Lett.* **2008**, *92*, 173303.

38. Hamwi, S.; Riedl, T.; Kowalsky, W. An organic *p-i-n* homojunction as ultra violet light emitting diode and visible-blind photodiode in one. *Appl. Phys. Lett.* **2011**, *99*, 053301:1–053301:3.

39. Chan, C.K.; Amy, F.; Zhang, Q.; Barlow, S.; Marder, S.; Kahn, A. N-type doping of an electron-transport material by controlled gas-phase incorporation of cobaltocene. *Chem. Phys. Lett.* **2006**, *431*, 67–71.

40. Walzer, K.; Maennig, B.; Pfeiffer, M.; Leo, K. Highly efficient organic devices based on electrically doped transport layers. *Chem. Rev.* **2007**, *107*, 1233–1271.

41. Falkenberg, C.; Uhrich, C.; Olthof, S.; Maennig, B.; Riede, M.; Leo, K. Efficient *p-i-n* type organic solar cells incorporating 1,4,5,8-naphthalenetetracarboxylic dianhydride as transparent electron transport material. *J. Appl. Phys.* **2008**, *104*, 034506:1–034506:6.

42. Yoshida, H. Low-energy inverse photoemission spectroscopy using a high-resolution grating spectrometer in the near ultraviolet range. *Rev. Sci. Instrum.* **2013**, *84*, 103901:1–103901:5.

43. Kubo, M.; Iketaki, K.; Kaji, T.; Hiramoto, M. Conduction type control of fullerene films from n- to p-type by molybdenum oxide doping. *Appl. Phys. Lett.* **2011**, *98*, 073311:1–073311:3.

44. Kubo, M.; Kaji, T.; Hiramoto, M. *pn*-homojunction formation in single fullerene films. *AIP Adv.* **2011**, *1*, 032177:1–032177:5.

45. Ishiyama, N.; Ishiyama, K.; Kubo, M.; Kaji, T.; Hiramoto, M. Tandem photovoltaic cells formed in single fullerene films by impurity doping. *Appl. Phys. Lett.* **2012**, *101*, 233303:1–233303:3.

46. Shinmura, Y.; Kubo, M.; Ishiyama, N.; Kaji, T.; Hiramoto, M. *pn*-control and *pn*-homojunction formation of metal-free phthalocyanine by doping. *AIP Adv.* **2012**, *2*, 032145:1–032145:6.

47. Hamwi, S.; Meyer, J.; Winkler, T.; Riedl, T.; Kowalsky, W. *p*-type doping efficiency of MoO_3 in organic hole transport materials. *Appl. Phys. Lett.* **2009**, *94*, 253307:1–253307:3.

48. Ishiyama, N.; Kubo, M.; Kaji, T.; Hiramoto, M. Doping-based control of the energetic structure of photovoltaic co-deposited films. *Appl. Phys. Lett.* **2011**, *99*, 133301:1–133301:3.

49. Note: Hole concentration created by MoO_3-doping (5000 ppm) was cross-checked by capacitance-voltage measurements. Obtained value of 5×10^{17} cm^{-3} was consistent with that measured by Kelvin method (9.6×10^{17} cm^{-3}).

50. Hebard, A.F.; Hadon, R.C.; Fleming, R.M.; Kortan, A.R. Deposition and characterization of fullerene films. *Appl. Phys. Lett.* **1991**, *59*, 2109–2111.

51. Note: There is no evidence of Cs_2CO_3 dissociation during vacuum evaporation, since a single Cs_2CO_3 film is completely transparent.

52. Note: The radius of an electron orbital around a positively ionized donor can be calculated based on the equation expressing the Bohr radius (r) including the relative permittivity (ε) and the effective mass of an electron (m_n*), *i.e.*, $r = \varepsilon_0 \varepsilon h^2 / \pi m_n * e^2$.

53. Kröger, M.; Hamwi, S.; Meyer, J.; Riedl, T.; Kowalsky, W.; Kahn, A. P-type doping of organic wide band gap materials by transition metal oxides: A case-study on Molybdenum trioxide. *Org. Electron.* **2009**, *10*, 932–938.

54. deMello, J.C.; Tessler, N.; Graham, S.C.; Friend, R.H. Ionic space-charge effects in polymer light-emitting diodes. *Phys. Rev. B* **1998**, *57*, 12951–12963.

55. Hiramoto, M.; Tomioka, A.; Suemori, K.; Yokoyama, M. Formation of ohmic contacts to perylene molecular crystals. *Appl. Phys. Lett.* **2004**, *85*, 1852–1854.

56. Kubo, M.; Shinmura, Y.; Ishiyama, N.; Kaji, T.; Hiramoto, M. Invertible organic photovoltaic cells with heavily-doped organic/metal ohmic contacts. *Appl. Phys. Expr.* **2012**, *5*, 092302:1–092302:3.

57. Note: The inverse photovoltaic effect in Figure 22(d)(blue curve) can be attributed to the *p*-type Schottky junction formation at Ag/H_2Pc interface. Absence of C_{60} sensitivity of action spectrum of J_{sc} of inverse photocurrent showed that the inverse photocurrent was generated near H_2Pc/Ag electrode.

58. Kubo, M.; Kaji, T.; Hiramoto, M. *pn*-homojunction organic solar cells formed in the thick phase-separated co-deposited films by doping. *Appl. Phys. Lett.* **2013**, *103*, 263303:1–263303:4.

59. Kubo, M.; Shinmura, Y.; Ishiyama, N.; Kaji, T.; Hiramoto, M. Junction formation by doping in $H_2Pc:C_{60}$ co-evaporated films for solar cell application. *Mol. Cryst. Liq. Cryst.* **2013**, *581*, 13–17.

60. Ishiyama, N.; Kubo, M.; Kaji, T.; Hiramoto, M. Tandem organic solar cells formed in co-deposited films by doping. *Org. Electron.* **2013**, *14*, 1793–1796.

61. Hiramoto, M.; Suezaki, M.; Yokoyama, M. Effect of thin gold interstitial-layer on the photovoltaic properties of tandem organic solar cell. *Chem. Lett.* **1990**, 327–330.

62. Yuan, Y.; Huang, J.; Li, G. Intermediate layers in tandem organic solar cells. *Green* **2011**, *1*, 65–80.